

Joint Access Point Selection and Beamforming Design for Bistatic Backscatter Communication

Ahmet Kaplan, Diana P. M. Osorio, and Erik G. Larsson

Abstract—Future Internet-of-Things networks are envisioned to use small and cheap sensor nodes with extremely low power consumption to avoid the extensive use of batteries. To provide connectivity to a massive number of these nodes, backscatter communication (BC) is emerging as an energy- and cost-efficient technology exploiting the reflection of radio frequency signals. However, challenges such as round-trip path loss and direct link interference (DLI) between the carrier emitter and the reader limit its performance. To tackle these limitations, this paper proposes a joint access point role selection and a novel beamforming technique for bistatic BC in a distributed multiple-input multiple-output setup. The proposed approach boosts the received backscattered energy while effectively mitigating DLI, thereby reducing the error probability. We also propose a channel estimation method tailored to operate under DLI conditions and propose a mismatch detector using estimated channel coefficients. Furthermore, we derive a closed-form expression for the probability of error for the detectors and model the quantization noise caused by DLI. Finally, comprehensive simulation results show that the proposed method with 1-bit analog-to-digital converters (ADCs) effectively mitigates DLI, reduces the quantization noise, and enhances backscattered signal energy, achieving performance comparable to the benchmark scenario with 8-bit ADCs.

Index Terms—Access point selection, bistatic backscatter communication, beamforming, direct link interference, internet of things

I. INTRODUCTION

Internet-of-Things (IoT) technology spans critical sectors such as healthcare, surveillance, and agriculture. Passive IoT devices offer a low-cost and sustainable solution by harnessing energy from ambient sources, such as radio frequency (RF) signals, thus eliminating the need for batteries. A key communication technology for passive IoT devices is backscatter communication (BC), which enables connectivity without requiring an active circuit to generate an RF signal [2]. Instead, passive devices modulate incoming RF signals by changing their phase and amplitude to transmit information.

A BC consists of three main components, namely carrier emitter (CE), reader, and backscatter device (BD). The CE transmits the carrier signal, while the reader receives the backscattered signal from the BD. Moreover, three types of operation are possible, monostatic BC (MoBC), bistatic BC (BiBC), and ambient BC (AmBC). In MoBC, the reader and carrier emitter are collocated; while in BiBC, the CE and reader are spatially separated, thus eliminating the need for full-duplex

operation [3], [4]. AmBC is similar to BiBC, but does not have dedicated CE and the BD reflects incoming ambient RF signals, such as Bluetooth or Wi-Fi [5]. Herein, we will focus on BiBC while addressing interested readers to find further details in comprehensive surveys on BC in [2], [6]–[10].

A. Motivation

The performance of BC can be significantly degraded due to two major problems, the round-trip path loss and the direct link interference (DLI). Due to the cascade channel, BC experiences round-trip path loss, which weakens the backscattered signal. Moreover, the weak BC signal received at the reader is strongly interfered by the carrier signal transmitted by the CE, which is called DLI. As a result, maintaining reliable communication becomes increasingly challenging as distances grow.

As a consequence of these problems, the dynamic range of the received signal (power ratio of the DLI to the BD signal) is too high, thus high resolution analog-to-digital converters (ADCs) are required in the reader circuitry. However, ADCs are power-hungry components, especially in multiple antenna technology, where each antenna requires its own ADC.

In light of these circumstances, BiBC offers key advantages including spatial separation of the CE and reader, unlike MoBC, and support for transmit beamforming (BF) with multiple antennas, unlike AmBC. For the aforementioned reasons, this paper investigates the benefits of distributed multiple-input multiple-output (MIMO) technology to enhance BiBC by deploying multiple access points (APs) across a geographic area. With spatial distributed APs, the round-trip path loss can be reduced due to macro diversity gain, thus allowing for extended range, increased data rates, improved interference management, and scalability for passive IoT devices.

B. Related Work

This subsection reviews related literature considering two main categories of works, i) BiBC with multi-antenna technology and ii) DLI cancellation in BiBC systems.

1) BiBC with multi-antenna technology

The works in [11]–[13] propose novel channel estimation algorithms for multi-antenna BiBC. Particularly, the work in [11] optimizes the sum rate by employing BF and multiple BDs. In [12], the signal-to-noise ratio (SNR) in a multi-antenna reader is maximized using the channel estimates in a BiBC setup with multi-antenna CE and a single antenna tag. In [13], the proposed approach allows for the estimation of the channels of several BDs in one shot in a BiBC setup with a multi-antenna reader.

Rate optimization is explored in [14]–[16] for the BiBC setup

with multi-antenna CE and multi-antenna reader. For instance, [14] proposes the maximization of the minimum rate of multiple BDs. The achievable rate with a CE transmitting information to a reader is investigated in [15]. In [16], deep reinforcement learning technique is employed to maximize the BDs sum rate.

Power beacon placement to extend coverage in BiBC is studied in [17], while [18] examines network capacity and coverage with multiple BDs and power beacons (CEs). Moreover, space-time code design for BiBC and MoBC systems with multi-antenna reader, CE, and BD is investigated in [19].

Our previous work, in [20], explores AP role selection for a BiBC setup with distributed MIMO. Different from that work, this work introduces a channel estimation algorithm, proposes a BF design, and addresses the DLI problem.

2) DLI cancelation in BiBC

The works in [21]–[29] investigate the DLI cancellation in BiBC. Particularly, in [21], [22] and [23], the carrier frequency of the backscattered signal is shifted at the BD to separate the DLI and the weak BC signal in the reader. This technique may increase the complexity of the BD and requires additional frequency bands.

Moreover, in [24] and [25], coding in the BD is used to cancel the DLI in the reader in a single-input single-output (SISO) BiBC setup, but the interference cancellation occurs after the ADC in the digital domain, thus requiring a high resolution ADC. In [26], the DLI is first estimated in the digital domain and then subtracted from the received signal in a SISO BiBC setup, thus still requiring a high resolution ADC.

In [27], the effect of the DLI on the communication range is investigated in BiBC and AmBC. In [28], the effect of imperfect successive interference cancellation (SIC) is investigated in a SISO BiBC setup with a hybrid BD supporting both passive and active operations. In [30], the DLI is first estimated and then subtracted in the analog domain in a SISO BiBC.

In our previous work in [31], we propose a method to cancel the DLI in a BiBC setup using a multi-antenna CE and reader. That work assumes no prior information about the BD and focuses solely on DLI cancellation without considering the enhancement of the backscattered signal's power. In [1], we address both DLI cancellation and power focusing to the BD in a BiBC setup with multi-antenna CE and reader. However, those studies involve only two APs, namely a CE and a reader.

The summary of the literature on the DLI cancelation in BiBC is given in Table I.

C. Contributions

Different from the aforementioned works, this paper addresses the DLI cancellation while increasing the received backscattered energy by jointly performing AP selection and BF design in a distributed MIMO setup. To the best of our knowledge, no existing literature addresses the same setup and problem. Our contributions can be summarized as follows:

- For different scenarios, optimization problems are defined to effectively address the DLI and round-trip path loss in BiBC. We propose the joint AP selection and BF design to mitigate the DLI, enhance the received backscattered energy, and minimize the probability of error.

TABLE I: Comparison of Related Works on DLI Cancelation

Ref	Dist. MIMO	Mult. BD	Chn. Est.	AP Role Selection	Novel DLI Cancelation Algorithm
[1]					Transmit beamforming
[16]		✓			Imperfect SIC considered
[21], [22]					Frequency shift in BD
[23]		✓			Frequency shift in BD
[24], [25]					Coding in BD, requires high-res. ADC
[26]					Estimated and subtracted, requires high-res. ADC
[27]					DLI effect analysis
[28]					Imperfect SIC considered
[30]					Canceled in analog domain
[31]			✓		Transmit beamforming
This work	✓	✓	✓	✓	Transmit beamforming and AP role selection

- A channel estimation algorithm is designed to operate effectively under DLI conditions in a BiBC setup with distributed MIMO.
- We propose detectors for both perfect and imperfect channel state informations (CSIs) and derive closed-form expressions for the probability of error.
- The quantization noise due to DLI is modeled, and the performance of the joint AP selection and BF algorithm is analyzed under quantization noise.
- Simulation results demonstrate the superior performance of the proposed algorithms in canceling DLI, enhancing backscattered energy, and improving error probability, even with 1-bit ADCs, compared to benchmark methods that use higher-resolution ADCs and design beamforming vectors without addressing DLI.

Note that, in [1], perfect channel knowledge is assumed, the DLI constraint is not defined per receive antenna, and neither AP selection nor quantization noise modeling is addressed. In contrast, this paper introduces channel estimation, quantization noise modeling, a per-antenna DLI constraint, and a joint AP selection and BF algorithm for systems with multiple APs.

The remaining part of this paper is organized as follows. Sections II, III, and IV present the system model, the proposed channel estimation algorithm, and the detector design, respectively. Sections V, VI, and VII define the optimization problems for maximizing the received backscattered energy under different scenarios, describe the proposed BF algorithm, and introduce the AP selection strategy, respectively. Complexity analysis and numerical results are provided in Sections VIII and IX, respectively. Finally, Section X concludes the paper.

Notation: $(\cdot)^T$, $(\cdot)^H$, $(\cdot)^*$, $\text{Re}\{\cdot\}$, and $\text{Im}\{\cdot\}$ denote transpose, Hermitian transpose, conjugate, and real and imaginary parts, respectively. For a set \mathcal{S} , $|\cdot|$ denotes cardinality, and for a scalar, absolute value. $\text{Tr}\{\cdot\}$ is the trace operator. Bold letters represent matrices (capital) and vectors (lowercase), while italic letters represent scalars. $\|\mathbf{X}\|$ and $\|\mathbf{x}\|$ are the Frobenius and Euclidean norms, respectively. $[\mathbf{x}]_{i:j}$ represents elements from the i -th to the j -th position of the vector \mathbf{x} , while $[\mathbf{X}]_{i,j}$ is the element in the i -th row and j -th column of the matrix \mathbf{X} . The i -th element of \mathbf{x} is x_i . Note that all vectors are

A. Step 1: Channel Estimation Between the BD and AP_{ref}

In this step, AP_{ref} first sends the pilot signal and then estimates the cascade BC channel using the backscattered pilot signal. After this, \mathbf{h}_{ref} is estimated using the cascade channel estimate and the algorithm provided in [3].

When AP_{ref} transmits the pilot signal, the backscattered pilot signal received at AP_{ref} during the j' -th time slot is expressed as

$$\mathbf{Y}_{\text{ref},j'} = \gamma_{j'} \mathbf{h}_{\text{ref}} \mathbf{h}_{\text{ref}}^T \Phi_{\text{ref}} + \mathbf{W}_{\text{ref},j'}. \quad (3)$$

The least-squares (LS) estimate of the cascade channel $\mathbf{H}_{\text{ref}} = \mathbf{h}_{\text{ref}} \mathbf{h}_{\text{ref}}^T$ is given by

$$\hat{\mathbf{H}}_{\text{ref}} = \sum_{j'=1}^{J'} \frac{1}{J' \gamma_{j'}} \mathbf{Y}_{\text{ref},j'} \Phi_{\text{ref}}^H (\Phi_{\text{ref}} \Phi_{\text{ref}}^H)^{-1}. \quad (4)$$

For the estimation of \mathbf{h}_{ref} , we follow the same steps as in [3], where a real symmetric matrix, $\check{\mathbf{G}} \in \mathbb{R}^{2M_{\text{ref}} \times 2M_{\text{ref}}}$, with real eigenvalues is formed by defining $\check{\mathbf{H}} \triangleq (\hat{\mathbf{H}}_{\text{ref}} + \hat{\mathbf{H}}_{\text{ref}}^*)/2$ and expressing it as

$$\check{\mathbf{G}} \triangleq \begin{bmatrix} \text{Re} \left\{ \check{\mathbf{H}} \right\} & -\text{Im} \left\{ \check{\mathbf{H}} \right\} \\ -\text{Im} \left\{ \check{\mathbf{H}} \right\} & -\text{Re} \left\{ \check{\mathbf{H}} \right\} \end{bmatrix}. \quad (5)$$

The real and imaginary parts of \mathbf{h}_{ref} are then estimated as

$$\begin{bmatrix} \text{Re} \left\{ \hat{\mathbf{h}}_{\text{ref}} \right\} \\ \text{Im} \left\{ \hat{\mathbf{h}}_{\text{ref}} \right\} \end{bmatrix} \triangleq \pm \sqrt{\lambda_{\check{\mathbf{G}}_1}} \frac{\mathbf{q}_{\check{\mathbf{G}}_1}}{\|\mathbf{q}_{\check{\mathbf{G}}_1}\|} \in \mathbb{R}^{2M_{\text{ref}} \times 1}, \quad (6)$$

where $\lambda_{\check{\mathbf{G}}_1}$ is the maximum eigenvalue of $\check{\mathbf{G}}$, and $\mathbf{q}_{\check{\mathbf{G}}_1}$ is the corresponding eigenvector. Finally, the estimate of \mathbf{h}_{ref} is

$$\hat{\mathbf{h}}_{\text{ref}} = \text{Re} \left\{ \hat{\mathbf{h}}_{\text{ref}} \right\} + j \text{Im} \left\{ \hat{\mathbf{h}}_{\text{ref}} \right\}. \quad (7)$$

Note that there can be 180-degree phase ambiguity in the estimate of \mathbf{h}_{ref} , but this does not affect the performance as shown in the next subsection.

B. Step 2: Channel Estimation Between the BD and the Remaining APs

In this step, we estimate \mathbf{h}_l ($\forall l \in \mathcal{L} \setminus \text{ref}$) using $\hat{\mathbf{h}}_{\text{ref}}$ and $\mathbf{Y}_{l,j'}$. First, the cascade BC channel is estimated using the ML algorithm as follows

$$\widehat{\mathbf{h}}_{\text{ref}} \hat{\mathbf{h}}_l^T = \sum_{j'=1}^{J'} \frac{1}{J' \gamma_{j'}} \mathbf{Y}_{l,j'} \Phi_l^H (\Phi_l \Phi_l^H)^{-1}. \quad (8)$$

Next, the estimate of \mathbf{h}_l is calculated as

$$\hat{\mathbf{h}}_l^T = \frac{\hat{\mathbf{h}}_{\text{ref}}^H}{\|\hat{\mathbf{h}}_{\text{ref}}\|^2} \widehat{\mathbf{h}}_{\text{ref}} \hat{\mathbf{h}}_l^T, \quad (9)$$

where $l \in \mathcal{L} \setminus \text{ref}$. The estimate of each \mathbf{h}_l is exposed to the same phase change coming from $\hat{\mathbf{h}}_{\text{ref}}$, as seen in (9). Since there is no phase mismatch between different APs, multiple APs can be used for coherent operations.

C. Step 3: Refinement of the Estimation of \mathbf{h}_{ref}

In Step 1, \mathbf{h}_{ref} is estimated using $\mathbf{Y}_{\text{ref},j'}$. However, the initial estimate of \mathbf{h}_{ref} can be refined using all received pilot signals, i.e., $\mathbf{Y}_{l,j'}$. Consequently, the initial estimate of \mathbf{h}_l in Step 2 can also be refined using the improved estimate of \mathbf{h}_{ref} .

Algorithm 1 Gradient Descent for Estimating \mathbf{h}_{ref}

Input: $\mathbf{Z}_{l,j'}$, initial estimate $\hat{\mathbf{h}}_{\text{ref}}$, estimates $\hat{\mathbf{h}}_l$, learning rate α_{lr} , maximum iteration T , and tolerance ϵ .

- 1: **Initialize:** Set $\mathbf{h}_{\text{ref}}^{(0)} = \hat{\mathbf{h}}_{\text{ref}}$ and $\nabla \mathcal{P}(\mathbf{h}_{\text{ref}}^{(-1)}) = 0$.
- 2: **for** $t \leftarrow 1$ to T **do**
- 3: Compute the gradient of the objective function: $\nabla \mathcal{P}(\mathbf{h}_{\text{ref}}^{(t-1)})$.
- 4: $\mathbf{h}_{\text{ref}}^{(t)} = \mathbf{h}_{\text{ref}}^{(t-1)} - \alpha_{lr} \left(\nabla \mathcal{P}(\mathbf{h}_{\text{ref}}^{(t-1)}) \right)^*$ [32, Ch. 8].
- 5: If $\left\| \nabla \mathcal{P}(\mathbf{h}_{\text{ref}}^{(t-1)}) - \nabla \mathcal{P}(\mathbf{h}_{\text{ref}}^{(t-2)}) \right\|^2 < \epsilon$, stop.
- 6: **end for**

Output: Estimated channel vector $\hat{\mathbf{h}}_{\text{ref}} = \mathbf{h}_{\text{ref}}^{(t)}$.

Once all pilot signals are received, and we have the estimation of $\hat{\mathbf{h}}_l$ s, we can refine the estimation of \mathbf{h}_{ref} by formulating the estimation problem as [31]

$$\hat{\mathbf{h}}_{\text{ref}} = \arg \min_{\mathbf{h}_{\text{ref}}} \left(\sum_{j'=1}^{J'} \left\| \frac{\mathbf{Y}_{\text{ref},j'} \Phi_{\text{ref}}^H}{\gamma_{j'} \alpha_{\text{ref}}} - \mathbf{h}_{\text{ref}} \mathbf{h}_{\text{ref}}^T \right\|^2 + \sum_{l \in \mathcal{L} \setminus \text{ref}} \sum_{j'=1}^{J'} \left\| \frac{\mathbf{Y}_{l,j'} \Phi_l^H}{\gamma_{j'} \alpha_l} - \mathbf{h}_{\text{ref}} \hat{\mathbf{h}}_l^T \right\|^2 \right). \quad (10)$$

To simplify the notation we define $\mathbf{Z}_{l,j'} \triangleq \mathbf{Y}_{l,j'} \Phi_l^H / (\gamma_{j'} \alpha_l)$. This estimation problem can be solved by using gradient descent (GD) with the initial estimate of \mathbf{h}_{ref} from Step 1 as an initial vector. The details are given in Algorithm 1, where the gradient of the objective function in (10) with respect to \mathbf{h}_{ref} is calculated as [33]

$$\begin{aligned} \nabla \mathcal{P}(\mathbf{h}_{\text{ref}}) &= \sum_{j'=1}^{J'} 2 \|\mathbf{h}_{\text{ref}}\|^2 \mathbf{h}_{\text{ref}}^* - (\mathbf{Z}_{\text{ref},j'}^* + \mathbf{Z}_{\text{ref},j'}^H) \mathbf{h}_{\text{ref}} \\ &+ \sum_{l \in \mathcal{L} \setminus \text{ref}} \sum_{j'=1}^{J'} \left\| \hat{\mathbf{h}}_l \right\|^2 \mathbf{h}_{\text{ref}}^* - \mathbf{Z}_{l,j'}^* \hat{\mathbf{h}}_l. \end{aligned} \quad (11)$$

D. Step 4: Iteration of Steps 2 and 3

To improve the channel estimates, we repeatedly perform Steps 2 and 3 until either the squared norm of the difference between the last two estimates of \mathbf{h}_{ref} falls below a small threshold or a pre-determined maximum number of iterations, ζ_{chn} , is reached. To ensure robustness against divergence, if the maximum iteration limit is reached, the final estimates $\hat{\mathbf{h}}_{\text{ref}}$ and $\hat{\mathbf{h}}_l$ are selected from the iteration i^* that gives the minimum value of the objective function $f(\hat{\mathbf{h}}_{\text{ref}}^{(i)}, \hat{\mathbf{h}}_l^{(i)})$, where $i \in \{0, 1, \dots, \zeta_{\text{chn}}\}$.

Algorithm 2 summarizes the channel estimation algorithm. The total pilot overhead is $J' \sum_{l=1}^L \tau_{p,l}$ symbols and it scales linearly with the number of APs. Note that the convergence of the Algorithm 2 to a global optimal point cannot be guaranteed due to the non-convex nature of the objective function in (2). However, the algorithm will converge to satisfactory estimates within a few iterations in practice when the SNR is moderate to high due to the accurate initial estimates.

Algorithm 2 Proposed Channel Estimation Procedure**Input:** $\mathbf{Y}_{l,j'}, \Phi_l, \gamma_{j'}, \epsilon, \zeta_{\text{chn}}$

- 1: Estimate initial $\hat{\mathbf{h}}_{\text{ref}}^{(0)}$ using $\mathbf{Y}_{\text{ref},j'}$ as in Step 1
- 2: For each AP $l \in \mathcal{L} \setminus \text{ref}$ estimate $\hat{\mathbf{h}}_l^{(0)}$ using $\hat{\mathbf{h}}_{\text{ref}}^{(0)}$ as in (9)
- 3: Set iteration counter $i \leftarrow 0$
- 4: **repeat**
- 5: $i \leftarrow i + 1$
- 6: Estimate $\hat{\mathbf{h}}_{\text{ref}}^{(i)}$ using $\hat{\mathbf{h}}_l^{(i-1)}$ and Algorithm 1
- 7: For each AP $l \in \mathcal{L} \setminus \text{ref}$ estimate $\hat{\mathbf{h}}_l^{(i)}$ using $\hat{\mathbf{h}}_{\text{ref}}^{(i)}$ as in (9)
- 8: **until** $\|\hat{\mathbf{h}}_{\text{ref}}^{(i)} - \hat{\mathbf{h}}_{\text{ref}}^{(i-1)}\|^2 < \epsilon$ or $i = \zeta_{\text{chn}}$
- 9: **if** $i = \zeta_{\text{chn}}$ **then**
- 10: **Output:** Estimates $\hat{\mathbf{h}}_{\text{ref}}, \hat{\mathbf{h}}_l$ minimizing $f(\hat{\mathbf{h}}_{\text{ref}}^{(i)}, \hat{\mathbf{h}}_l^{(i)})$ over $i \in \{0, \dots, \zeta_{\text{chn}}\}$
- 11: **else**
- 12: **Output:** $\hat{\mathbf{h}}_{\text{ref}} = \hat{\mathbf{h}}_{\text{ref}}^{(i)}, \hat{\mathbf{h}}_l = \hat{\mathbf{h}}_l^{(i)}$
- 13: **end if**

E. Special Case, $M_{\text{ref}} = 1$

For $M_{\text{ref}} = 1$, the estimation of h_{ref} can be simplified to

$$\hat{h}_{\text{ref}} = \sqrt{\hat{H}_{\text{ref}}} = \sqrt{|\hat{H}_{\text{ref}}| e^{j\varphi}} = \sqrt{|\hat{H}_{\text{ref}}|} e^{j\varphi/2}, \quad (12)$$

where \hat{H}_{ref} , a complex scalar, is calculated using (4). Next, the estimate of \mathbf{h}_l is calculated as in Section III-B. Using (11), one can show that $\nabla \mathcal{P}(\hat{h}_{\text{ref}}) = 0$, making these estimates optimal. Therefore, there is no need to apply Step 3 and Step 4 of the proposed channel estimation algorithm in this special case.

F. Multiple BDs Case

In the case of multiple BDs, the received pilot signal in (1) contains the superposition of all reflected signals from different BDs, $\sum_k \gamma_{j',k} \mathbf{h}_{\text{ref}}^k (\mathbf{h}_l^k)^T \Phi_l$. To estimate the channels associated with the k -th BD, the channel estimation procedure must be repeated using the reflection coefficient sequence of the k -th BD, i.e., $\gamma_{j',k}$. Note that $J' \geq K$ to satisfy the orthogonality condition. For example, to estimate $\mathbf{h}_{\text{ref}}^k$ and $\mathbf{h}_{\text{ref}}^k (\mathbf{h}_l^k)^T$, $\gamma_{j',k}$ should be used in the computations of (4) and (8), respectively. Similarly, in (11), $\gamma_{j',k}$ must be used to estimate $\mathbf{h}_{\text{ref}}^k$. In summary, the channel estimation steps can be repeated per BD due to the orthogonal reflection coefficients.

IV. PROPOSED DETECTOR AND PROBABILITY OF ERROR

In this section, we first model the quantization error in the output of ADCs in the reader circuitry. Then, we define the hypothesis testing problem considering quantization noise and propose the maximum a posteriori probability (MAP) detector to detect the information bits from the BD for both imperfect and perfect CSI cases. In addition, we derive the probability of error expressions for the proposed detector under both cases.

A. Modeling of Quantization Noise

We assume that each antenna has two ADCs, one for the in-phase component and one for the quadrature-phase component. Each ADC uses a uniform mid-rise quantization. The nonlinear quantization function $Q(y)$ maps the real-valued input $y \in \mathbb{R}$

to one of the quantization levels, and Δ which is the the quantization step size is adjusted as

$$\Delta = \sqrt{\mathbb{E}\{y^2\}}/2^{b-1}. \quad (13)$$

The number of quantization levels is 2^b , where b is the number of bits in ADCs.

The quantization noise is defined as $n = Q(y) - y$. If y is Gaussian, n is uniformly distributed with the variance approximated as $\mathbb{E}\{n^2\} = \sigma_n^2 \approx \Delta^2/12$ [34]. For analytic tractability, we assume that the quantization noise follows a zero-mean Gaussian distribution, denoted as $\mathcal{N}(0, \sigma_n^2)$. When the input to the quantization function is a vector, the function is applied element-wise, and the elements of the quantization noise are assumed to be independently distributed $\mathcal{N}(0, \sigma_n^2)$. While the quantization noise may exhibit spatial correlation, as each receive antenna observes a different linear combination of the same transmitted signal, we follow i.i.d. Gaussian assumption to simplify the analysis [35], [36]. This approximation is also accurate in the low-SNR region.

For BC, we model the quantizer input y as $y = x + i + w$, where x is the desired backscattered signal, i is the DLI originating from the direct path between the transmitter and receiver, and w is the additive noise term. The signal-to-quantization noise ratio is defined as

$$\text{SQNR} = \frac{\mathbb{E}\{x^2\}}{\mathbb{E}\{n^2\}} \approx \frac{3 \times 2^{2b} \mathbb{E}\{x^2\}}{\mathbb{E}\{y^2\}}, \quad (14)$$

which increases by 6.02 dB for each additional bit in the ADCs. In addition, the dynamic range of a b -bit ADC is defined as the ratio of the largest to the smallest change in the output signal, i.e., $\Delta(2^b - 1)/\Delta$, and can be approximated as 6.02b dB [37].

It is observed from (13) that the quantization step size increases with stronger interference. This rise in the quantization step increases the variance of the quantization noise, reducing SQNR in (14), and consequently, communication performance will be significantly degraded in the presence of strong interference.

B. Hypothesis Testing

The hypothesis testing problem, which accounts for the effects of quantization noise on detecting BD information bits, is formulated using two hypotheses: \mathcal{H}_0 and \mathcal{H}_1 . These hypotheses correspond to the cases where the transmitted bit is “0” and “1”, respectively, and given by

$$\mathcal{H}_i : \mathbf{y}_j = Q(\mathbf{H}_{\text{DL}} \mathbf{x} + \gamma_j^i \mathbf{H}_{\text{BL}} \mathbf{x} + \mathbf{w}_j), \quad (15)$$

where $i \in \{0, 1\}$. The function $Q(\cdot)$ is applied to the real and the imaginary parts of the input signal separately. The vector $\mathbf{y}_j \in \mathbb{C}^{N_{\text{R}} \times 1}$ is the received signal at the readers in the j -th time slot ($j = 1, \dots, J$) and \mathbf{x} is the beamforming vector showing the transmitted signal from all the CEs. The beamformer \mathbf{x} is designed to enhance the BC performance in the presence of DLI, and its design is detailed in Sections V and VI. The scalar γ_j^i shows the reflection coefficient of the BD in time slot j under hypothesis \mathcal{H}_i . For simplicity, we assume that $|\gamma_j^i|^2 = \delta, \forall i, j$, where δ is a constant. The vector $\mathbf{w}_j \in \mathbb{C}^{N_{\text{R}} \times 1}$ is the additive Gaussian noise and all its elements are i.i.d. $\mathcal{CN}(0, 1)$.

Considering quantization, the hypotheses become

$$\mathcal{H}_i : \mathbf{y}_j = \mathbf{H}_{\text{DL}}\mathbf{x} + \gamma_j^i \mathbf{H}_{\text{BL}}\mathbf{x} + \mathbf{w}_j + \mathbf{n}_j, \quad (16)$$

where \mathbf{n}_j stands for the quantization noise after ADC, and its elements follow independent Gaussian distribution. The r -th element of \mathbf{n}_j , i.e., $n_{j,r}$, is modeled as $\mathcal{CN}(0, \sigma_{j,r}^2)$ with the variance given by

$$\sigma_{j,r}^2 = \left(\mathbb{E} \left\{ \left| \mathbf{h}_{\text{DL},r}^\top \mathbf{x} \right|^2 \right\} + \mathbb{E} \left\{ \left| \delta \mathbf{h}_{\text{BL},r}^\top \mathbf{x} \right|^2 \right\} + 1 \right) / (2^{2b_r} \times 3), \quad (17)$$

where $r = 1, \dots, N_R$, and $\mathbf{h}_{\text{BL},r}^\top \in \mathbb{C}^{1 \times N_C}$ and $\mathbf{h}_{\text{DL},r}^\top \in \mathbb{C}^{1 \times N_C}$ are the r -th rows of \mathbf{H}_{BL} and \mathbf{H}_{DL} , respectively. The variable b_r denotes the resolution of the ADC associated with the receive antenna corresponding to the r -th row of \mathbf{H}_{BL} . The covariance matrix of $\mathbf{w}_j + \mathbf{n}_j$ is defined as $N_R \times N_R$ diagonal matrix $\mathbf{D}_j = \text{diag}(\sigma_{j,1}^2 + 1, \dots, \sigma_{j,N_R}^2 + 1)$.

C. Perfect CSI

In this subsection, we assume perfect CSI and derive the optimal MAP detector and its probability of error.¹ Assuming $P(\mathcal{H}_0) = P(\mathcal{H}_1) = 1/2$, the optimal MAP detector is

$$\frac{\prod_j p(\mathbf{y}_j | \mathcal{H}_1)}{\prod_j p(\mathbf{y}_j | \mathcal{H}_0)} \underset{\mathcal{H}_0}{\overset{\mathcal{H}_1}{\gtrless}} 1, \quad (18)$$

where $p(\mathbf{y}_j | \mathcal{H}_i)$ is the probability density function (pdf) of the received signal under \mathcal{H}_i , and it is expressed as

$$p(\mathbf{y}_j | \mathcal{H}_i) = \frac{1}{\pi^{N_R} \det(\mathbf{D}_j)} \exp \left[- \left\| \mathbf{D}_j^{-1/2} (\mathbf{y}_j - \mathbf{H}_{\text{DL}}\mathbf{x} - \gamma_j^i \mathbf{H}_{\text{BL}}\mathbf{x}) \right\|^2 \right]. \quad (19)$$

We first define $\mathbf{y}'_j = \mathbf{y}_j - \mathbf{H}_{\text{DL}}\mathbf{x}$, and then substitute the pdfs into (18). Then, by taking the logarithm of both sides in (18), the detector can be expressed as

$$\sum_j \left\{ \left\| \mathbf{D}_j^{-1/2} (\mathbf{y}'_j - \gamma_j^0 \mathbf{H}_{\text{BL}}\mathbf{x}) \right\|^2 - \left\| \mathbf{D}_j^{-1/2} (\mathbf{y}'_j - \gamma_j^1 \mathbf{H}_{\text{BL}}\mathbf{x}) \right\|^2 \right\} \underset{\mathcal{H}_0}{\overset{\mathcal{H}_1}{\gtrless}} 0. \quad (20)$$

Using the identity $\|\mathbf{a} - \mathbf{b}\|^2 = \|\mathbf{a}\|^2 + \|\mathbf{b}\|^2 - 2 \text{Re} \{ \mathbf{a}^H \mathbf{b} \}$ and $|\gamma_j^i|^2 = \delta, \forall i, j$, the detector can be re-expressed as follows

$$\text{LLR} = \sum_j \text{Re} \left\{ (\gamma_j^1 - \gamma_j^0) \mathbf{y}'_j{}^H \mathbf{D}_j^{-1} \mathbf{H}_{\text{BL}}\mathbf{x} \right\} \underset{\mathcal{H}_0}{\overset{\mathcal{H}_1}{\gtrless}} 0, \quad (21)$$

where LLR is the test statistic. Under \mathcal{H}_i , the test statistic is

$$\begin{aligned} \text{LLR} &= \sum_j \text{Re} \left\{ (\gamma_j^1 - \gamma_j^0) (\gamma_j^i)^* \right\} \left\| \mathbf{D}_j^{-1/2} \mathbf{H}_{\text{BL}}\mathbf{x} \right\|^2 \\ &+ \text{Re} \left\{ (\gamma_j^1 - \gamma_j^0) (\mathbf{w}_j + \mathbf{n}_j)^H \mathbf{D}_j^{-1} \mathbf{H}_{\text{BL}}\mathbf{x} \right\}. \end{aligned} \quad (22)$$

¹While the detector structure is conventional, incorporating quantization noise into the analysis and deriving the probability of error are crucial for evaluating the performance under realistic low-resolution conditions.

The distribution of the test statistic under \mathcal{H}_i is

$$\begin{aligned} \text{LLR} &\sim \mathcal{N} \left(\sum_j \text{Re} \left\{ (\gamma_j^1 - \gamma_j^0) (\gamma_j^i)^* \right\} \left\| \mathbf{D}_j^{-1/2} \mathbf{H}_{\text{BL}}\mathbf{x} \right\|^2, \right. \\ &\left. \sum_j \frac{|\gamma_j^1 - \gamma_j^0|^2}{2} \left\| \mathbf{D}_j^{-1/2} \mathbf{H}_{\text{BL}}\mathbf{x} \right\|^2 \right). \end{aligned} \quad (23)$$

The probability of error is $P_e = P(\mathcal{H}_0)P(\mathcal{H}_1|\mathcal{H}_0) + P(\mathcal{H}_1)P(\mathcal{H}_0|\mathcal{H}_1)$, and it is calculated as²

$$P_e \stackrel{(a)}{=} Q \left(\left\| \mathbf{D}_j^{-1/2} \mathbf{H}_{\text{BL}}\mathbf{x} \right\| \sqrt{\sum_j \frac{|\gamma_j^1 - \gamma_j^0|^2}{2}} \right), \quad (24)$$

where $Q(x) = \frac{1}{\sqrt{2\pi}} \int_x^\infty \exp(-\frac{u^2}{2}) du$. In (a), we use the equality $\text{Re} \{ -(\gamma_j^1 - \gamma_j^0) (\gamma_j^0)^* \} = |\gamma_j^1 - \gamma_j^0|^2 / 2$. For infinite resolution ADCs, \mathbf{D}_j is an identity matrix, and the probability of error is defined as P_e^{inf} . It can be showed $P_e^{\text{inf}} \leq P_e$ because each diagonal element of $\mathbf{D}_j^{-1/2}$ is less than or equal to 1 in P_e .

D. Imperfect CSI

When there is no perfect CSI, the estimated channel coefficients are used in a mismatch detector which can be expressed similarly to (21) as

$$\sum_j \text{Re} \left\{ (\gamma_j^1 - \gamma_j^0) \hat{\mathbf{y}}_j{}^H \hat{\mathbf{D}}_j^{-1} \hat{\mathbf{H}}_{\text{BL}}\mathbf{x} \right\} \underset{\mathcal{H}_0}{\overset{\mathcal{H}_1}{\gtrless}} 0, \quad (25)$$

where $\hat{\mathbf{y}}'_j = \mathbf{y}_j - \hat{\mathbf{H}}_{\text{DL}}\mathbf{x}$, $\hat{\mathbf{H}}_{\text{BL}} = \hat{\mathbf{h}}_R \hat{\mathbf{h}}_C^T$ and $\hat{\mathbf{D}}_j$ is created using the estimated CSI instead of perfect CSI in (17).

Under \mathcal{H}_i , the test statistic is given by

$$\begin{aligned} \text{LLR}' &= \sum_j \text{Re} \left\{ (\gamma_j^1 - \gamma_j^0) \right. \\ &\left. (\gamma_j^i \mathbf{H}_{\text{BL}}\mathbf{x} + \mathbf{E}_{\text{DL}}\mathbf{x} + \mathbf{w}_j + \mathbf{n}_j)^H \hat{\mathbf{D}}_j^{-1} \hat{\mathbf{H}}_{\text{BL}}\mathbf{x} \right\}, \end{aligned} \quad (26)$$

where \mathbf{E}_{DL} models the channel estimation error for \mathbf{H}_{DL} , and each element of it is assumed to have i.i.d. $\mathcal{CN}(0, \sigma_{\text{DL}}^2)$. Therefore, each element of the vector $\mathbf{E}_{\text{DL}}\mathbf{x}$ follows i.i.d. $\mathcal{CN}(0, \|\mathbf{x}\|^2 \sigma_{\text{DL}}^2)$ and $\|\mathbf{x}\|^2 \sigma_{\text{DL}}^2 \mathbf{I}_{N_R}$ is the covariance matrix of $\mathbf{E}_{\text{DL}}\mathbf{x}$. The mean under \mathcal{H}_i and the variance of the test statistic are calculated, respectively, as follows

$$\begin{aligned} \mu_{\text{LLR}'|\mathcal{H}_i} &= \sum_j \text{Re} \left\{ (\gamma_j^1 - \gamma_j^0) (\gamma_j^i \mathbf{H}_{\text{BL}}\mathbf{x})^H \hat{\mathbf{D}}_j^{-1} \hat{\mathbf{H}}_{\text{BL}}\mathbf{x} \right\}, \\ \sigma_{\text{LLR}'}^2 &= \frac{1}{2} \sum_j |\gamma_j^1 - \gamma_j^0|^2 \left\| \mathbf{C}_j \hat{\mathbf{H}}_{\text{BL}}\mathbf{x} \right\|^2, \end{aligned} \quad (27)$$

where $\mathbf{C}_j = \left(\hat{\mathbf{D}}_j^{-1} (\mathbf{D}_j + \mathbf{I}_{N_R} \|\mathbf{x}\|^2 \sigma_{\text{DL}}^2) \hat{\mathbf{D}}_j^{-1} \right)^{1/2} \in \mathbb{R}^{N_R \times N_R}$ is a diagonal matrix. As a result, the distribution of the test statistic under \mathcal{H}_i is $\text{LLR}' \sim \mathcal{N}(\mu_{\text{LLR}'|\mathcal{H}_i}, \sigma_{\text{LLR}'}^2)$. The probability of error is

$$P_e = \frac{1}{2} Q \left(-\frac{\mu_{\text{LLR}'|\mathcal{H}_0}}{\sigma_{\text{LLR}'}} \right) + \frac{1}{2} Q \left(\frac{\mu_{\text{LLR}'|\mathcal{H}_1}}{\sigma_{\text{LLR}'}} \right). \quad (28)$$

Under perfect CSI, as shown in (20), the detector multiplies the received signal by $\mathbf{D}_j^{-1/2}$, weighting the contribution of each receive antenna according to the total noise variance.

²Note that the i.i.d. quantization noise assumption leads to approximate P_e values in high-SNR region.

The same weighting also appears in (24). This pre-whitening operation ensures that antennas with lower noise variance have a stronger influence on the detection outcome. However, in the case of imperfect CSI, the estimated $\hat{\mathbf{D}}_j^{-1}$ causes suboptimal noise equalization, as seen in (25), and this effect also appears in (28). Consequently, P_e degrades under imperfect CSI due to both suboptimal pre-whitening and channel estimation errors.

E. Multiple BDs Case

In the case of multiple BD, the hypotheses for the k -th BD are defined as

$$\mathcal{H}_i^k : \mathbf{y}_j = \mathbf{H}_{\text{DL}}\mathbf{x} + \gamma_{j,k}^i \mathbf{H}_{\text{BL}}^k \mathbf{x} + \sum_{k' \neq k} \gamma_{j,k'}^i \mathbf{H}_{\text{BL}}^{k'} \mathbf{x} + \mathbf{w}_j + \mathbf{n}_j, \quad (29)$$

where each BD uses an orthogonal reflection coefficient sequence, and $J \geq K$. Therefore, by using $\gamma_{j,k}^i$ in place of γ_j^i , one can show that the detectors in (21) and (25), as well as the error probability expressions in (24) and (28) remain valid for the k -th BD under the assumption that $|\gamma_{j,k}^i|^2 = \delta_k, \forall i, j$, where δ_k is a constant.

V. PROBLEM DEFINITIONS

As seen in (24), increasing $\|\mathbf{D}_j^{-1/2} \mathbf{H}_{\text{BL}} \mathbf{x}\|$ reduces P_e . While directly maximizing this term seems straightforward, it is highly sensitive to inaccuracies in the quantization noise model. Moreover, \mathbf{D}_j depends on both direct and backscatter channels, which may not be reliably known in practice. In addition, maximizing $\|\mathbf{D}_j^{-1/2} \mathbf{H}_{\text{BL}} \mathbf{x}\|$ is considerably more complicated than maximizing $\|\mathbf{H}_{\text{BL}} \mathbf{x}\|$ due to the dependence of \mathbf{D}_j on \mathbf{x} . To enhance robustness under such imperfections, we instead maximize $\|\mathbf{H}_{\text{BL}} \mathbf{x}\|$, and introduce a signal-to-interference ratio (SIR) constraint to suppress DLI and indirectly regulate \mathbf{D}_j .³

To maximize $\|\mathbf{H}_{\text{BL}} \mathbf{x}\|$ in BiBC over the distributed MIMO setup, we consider the joint AP role selection and BF vector design. This objective is formulated as an optimization problem under seven different scenarios. The first two scenarios do not impose any constraints on DLI, while the remaining scenarios include constraints to mitigate DLI. The details of each scenario are outlined in this section, and the proposed solutions are discussed in the following sections.

Note that AP selection directly affects the objective $\|\mathbf{H}_{\text{BL}} \mathbf{x}\|^2 = \|\mathbf{h}_R\|^2 |\mathbf{h}_C^T \mathbf{x}|^2$ by determining the channels \mathbf{h}_C and \mathbf{h}_R , thus influencing the backscattered signal power. In DLI-constrained problems, where \mathbf{x} lies in the null space of the direct-link channel, AP selection also shapes this null space, and enables a trade-off between suppressing DLI and maximizing $\|\mathbf{H}_{\text{BL}} \mathbf{x}\|^2$. Hence, optimizing AP selection is essential not only for maximizing signal power but also for enabling effective interference control.

³Nonetheless, it is possible to maximize $\|\mathbf{D}_j^{-1/2} \mathbf{H}_{\text{BL}} \mathbf{x}\|$, for example, using the fractional optimization method from [38]. The details are provided in the Appendix. The results show that the performance gain achieved by optimizing $\|\mathbf{D}_j^{-1/2} \mathbf{H}_{\text{BL}} \mathbf{x}\|^2$ instead of $\|\mathbf{H}_{\text{BL}} \mathbf{x}\|^2$ is minuscule.

A. Maximizing the Received Backscatter Energy

In this scenario, we do not consider the DLI constraint, thus the optimization problem can be formulated as

$$\mathcal{P}_{\text{BF}} : \underset{\mathbf{x} \in \mathbb{C}^{N_C \times 1}, \mathcal{S}}{\text{maximize}} \quad \|\mathbf{H}_{\text{BL}} \mathbf{x}\|^2 \quad (30a)$$

$$\text{subject to (s.t.) } \|\mathbf{x}\|^2 \leq P_{\text{max}}, \quad (30b)$$

$$\text{AP}_{\text{ref}} \in \mathcal{S}_R. \quad (30c)$$

The constraint (30b) limits the total transmitted energy, and (30c) guarantees that the AP_{ref} is in the reader set. Although the problem disregards DLI, except for the constraint (30c) helping to operate under DLI, it is expected that interference reduces compared to the case of omnidirectional radiation due to the focused energy on the BC link.

On the other hand, in practical systems, each antenna is equipped with its power amplifier. The transmitted energy per antenna can also be constrained to use power resources efficiently. In this case, a new formulation, \mathcal{P}'_{BF} , is defined by replacing constraint (30b) with $|x_c|^2 \leq P_{\text{max}}, c = 1, \dots, N_C$, where x_c is the c -th element of the vector \mathbf{x} .

B. DLI Cancellation

In the case of limitations on the dynamic range of the ADCs in the reader circuitry, we should consider SIR in the reader when designing the transmit beamforming vector to maximize the error performance in BiBC. This is because the dynamic range of the received signal, and consequently the quantization error, increases with the decreasing SIR_r in the r -th received antenna, which is expressed as

$$\text{SIR}_r = \frac{1}{\eta_r} = \frac{|\mathbf{h}_{\text{BL},r}^T \mathbf{x}|^2}{|\mathbf{h}_{\text{DL},r}^T \mathbf{x}|^2}, \quad (31)$$

where η_r is the dynamic range of the received signal in r -th received antenna.

Therefore, we formulate the problem \mathcal{P}_{DLI} as the maximization of the received backscattered energy subject to a constraint on the DLI, and it can be expressed as

$$\begin{aligned} \mathcal{P}_{\text{DLI}} : \underset{\mathbf{x} \in \mathbb{C}^{N_C \times 1}, \mathcal{S}}{\text{maximize}} \quad & \|\mathbf{H}_{\text{BL}} \mathbf{x}\|^2 \\ \text{s.t.} \quad & (30b), (30c), \frac{|\mathbf{h}_{\text{DL},r}^T \mathbf{x}|^2}{|\mathbf{h}_{\text{BL},r}^T \mathbf{x}|^2} \leq \alpha, \forall r/r_{\text{ref}}, \end{aligned} \quad (32)$$

where r_{ref} corresponds to the antenna indices of the AP_{ref} . The SIR at the antennas of the reference AP is excluded from the constraint, as these antennas are equipped with high-resolution ADCs. The required dynamic range of the ADCs in the reader is proportional to α . A reduction of 6 dB in α approximately corresponds to 6 dB increase in SQNR, given in (14), particularly in scenarios with strong DLI. Therefore, for each 6 dB reduction in α , the number of bits required in ADCs can be reduced by one while maintaining the same SQNR.

The choice of α depends on use-case requirements and reader ADC resolution. Increasing α increases received backscatter energy but also raises DLI. For large α , \mathcal{P}_{DLI} converges to \mathcal{P}_{BF} .

Alternatively, one can also limit the transmitted energy per antenna. In this case, the new problem $\mathcal{P}'_{\text{DLI}}$ is defined by replac-

TABLE II: Summary of the problems

Problem	Energy Constraint	DLI Constraint	BF Design
\mathcal{P}_{BF}	$\ \mathbf{x}\ ^2 \leq P_{\max}$	—	(37)
\mathcal{P}_{DLI}		$\eta_r \leq \alpha, \forall r/r_{\text{ref}}$	(43)
$\mathcal{P}_{\alpha 0}$		$\mathbf{H}'_{\text{DL}} \mathbf{x} = 0$	(46)
$\mathcal{P}_{\text{multi}}$		$\mathbf{H}'_{\text{DL}} \mathbf{x} = 0$	Section VI-F
\mathcal{P}'_{BF}	$ x_c ^2 \leq P_{\max}, \forall c$	—	(40)
$\mathcal{P}'_{\text{DLI}}$		$\eta_r \leq \alpha, \forall r/r_{\text{ref}}$	Section VI-C
$\mathcal{P}'_{\alpha 0}$		$\mathbf{H}'_{\text{DL}} \mathbf{x} = 0$	Section VI-E

ing constraint (30b) in \mathcal{P}_{DLI} with $|x_c|^2 \leq P_{\max}, c = 1, \dots, N_C$.

C. Complete DLI Cancellation

In this scenario, it is considered that DLI is completely mitigated, i.e. $\alpha = 0$, thus the DLI constraint in (32) can be written as $\mathbf{h}_{\text{DL},r}^T \mathbf{x} = 0, \forall r/r_{\text{ref}}$. This constraint can be simplified as $\mathbf{H}'_{\text{DL}} \mathbf{x} = 0$, which means that \mathbf{x} lies in the nullspace of \mathbf{H}'_{DL} , i.e., $\mathbf{x} \in N(\mathbf{H}'_{\text{DL}})$. The matrix $\mathbf{H}'_{\text{DL}} \in \mathbb{C}^{N_R - M_{\text{ref}} \times N_C}$ is obtained by removing the M_{ref} rows of \mathbf{H}_{DL} corresponding to the channel between the CEs and the AP_{ref}. Therefore, the optimization problem can be formulated as

$$\mathcal{P}_{\alpha 0} : \begin{aligned} & \underset{\mathbf{x} \in \mathbb{C}^{N_C \times 1}, \mathcal{S}}{\text{maximize}} && \|\mathbf{H}_{\text{BL}} \mathbf{x}\|^2 \\ & \text{s.t.} && (30\text{b}), (30\text{c}), \mathbf{x} \in N(\mathbf{H}'_{\text{DL}}). \end{aligned} \quad (33)$$

Alternatively, one can also limit the transmitted energy per antenna. In this case, the new problem $\mathcal{P}'_{\alpha 0}$ is defined by replacing constraint (30b) with $|x_c|^2 \leq P_{\max}, \forall c$.

D. Multiple BDs Case

For the multiple BDs case, we first define the signal-to-interference-plus-noise ratio (SINR) for the k -th BD as

$$\text{SINR}_k = \frac{\delta_k \left| \mathbf{u}_k^H \mathbf{H}_{\text{BL}}^k \mathbf{x} \right|^2}{\left| \mathbf{u}_k^H \mathbf{H}_{\text{DL}} \mathbf{x} \right|^2 + \sum_{k' \neq k} \delta_{k'} \left| \mathbf{u}_k^H \mathbf{H}_{\text{BL}}^{k'} \mathbf{x} \right|^2 + \|\mathbf{u}_k\|^2}, \quad (34)$$

where $\mathbf{H}_{\text{BL}}^k = \mathbf{h}_R^k (\mathbf{h}_C^k)^T$, $\mathbf{u}_k = \mathbf{h}_R^k$, and $\left| \gamma_{j,k}^i \right|^2 = \delta_k, \forall i, j$. The problem is defined as

$$\mathcal{P}_{\text{multi}} : \begin{aligned} & \underset{\mathbf{x} \in \mathbb{C}^{N_C \times 1}, \mathcal{S}}{\text{maximize}} \min_k && \text{SINR}_k \\ & \text{s.t.} && (30\text{b}), \mathbf{x} \in N(\mathbf{H}'_{\text{DL}}). \end{aligned} \quad (35)$$

Similar to the other problems, we exclude quantization noise from the SINR definition to improve the robustness of $\mathcal{P}_{\text{multi}}$ against modeling inaccuracies. We instead introduce a DLI constraint in the problem formulation.

Table II summarizes the optimization problems by comparing the transmitted energy and the DLI constraints. Additionally, it provides the corresponding equation numbers for the solutions for BF design for the given AP partitioning. The detailed solutions for both BF design and AP selection, for all scenarios, are presented in Sections VI and VII, respectively.

Note that, to isolate and focus on one of the dominant performance bottlenecks of BC, which is the quantization error due to the DLI in the reader, we assume ideal (high-resolution) DACs. This assumption maintains analytical tractability and allows the transmit vector \mathbf{x} to remain unconstrained. Unlike ADCs, DACs do not suffer from DLI, and precoding designs

with low-resolution DACs are well-studied in the literature [39], [40]. It has been shown that low-resolution DACs can approach the performance of ideal DACs [40]. In addition, phase-only BF design is more beneficial in the low-resolution DAC scenario, and $\mathcal{P}'_{\text{DLI}}$, whose optimal BF solution is approximately phase-only, is well suited for such scenarios.

VI. PROPOSED BEAMFORMING DESIGNS

In this section, we design the beamforming vector to maximize the received backscattered energy for a given set \mathcal{S} .

A. Beamforming Design for \mathcal{P}_{BF}

The problem \mathcal{P}_{BF} for the given set \mathcal{S} can be written as

$$\mathcal{P}_{\text{BF},1} : \underset{\mathbf{x} \in \mathbb{C}^{N_C \times 1}}{\text{maximize}} \mathbf{x}^H \mathbf{H}_{\text{BL}}^H \mathbf{H}_{\text{BL}} \mathbf{x}, \text{ s.t. } \|\mathbf{x}\|^2 \leq P_{\max}. \quad (36)$$

This problem is known as the Rayleigh quotient, and the optimal \mathbf{x} is the right singular vector of \mathbf{H}_{BL} , where $\text{rank}(\mathbf{H}_{\text{BL}}) = 1$. The optimal solution is

$$\mathbf{x}_{\text{BF}} = \sqrt{P_{\max}} \mathbf{v}_{\text{BL}} = \sqrt{P_{\max}} e^{j\theta} \mathbf{h}_C^* / \|\mathbf{h}_C\|, \quad (37)$$

where $\mathbf{v}_{\text{BL}} \in \mathbb{C}^{N_C \times 1}$ is the right singular vector with the unit norm and \mathbf{x}_{BF} corresponds to the maximum-ratio transmission (MRT). The term $e^{j\theta}$ represents a common phase rotation applied to all transmit antennas. The phase $\theta \in [0, 2\pi)$ does not affect the constructive summation of the transmitted signals at the reader, as the relative phase alignment between antennas remains unchanged. The solution is therefore not unique, and any constant phase shift θ yields the same performance.

B. Beamforming Design for \mathcal{P}'_{BF}

The problem \mathcal{P}'_{BF} for the given set \mathcal{S} can be written as

$$\mathcal{P}'_{\text{BF},1} : \underset{\mathbf{x} \in \mathbb{C}^{N_C \times 1}}{\text{maximize}} \left\| \sigma_{\text{BL}} \mathbf{u}_{\text{BL}} \mathbf{v}_{\text{BL}}^H \mathbf{x} \right\|^2, \text{ s.t. } |x_c|^2 \leq P_{\max}, \forall c, \quad (38)$$

where the singular value decomposition (SVD) of $\mathbf{H}_{\text{BL}} = \sigma_{\text{BL}} \mathbf{u}_{\text{BL}} \mathbf{v}_{\text{BL}}^H$ and $\mathbf{u}_{\text{BL}} \in \mathbb{C}^{N_R \times 1}$ has unit norm. The problem can be equivalently expressed as

$$\mathcal{P}'_{\text{BF},1} : \underset{\mathbf{x} \in \mathbb{C}^{N_C \times 1}}{\text{maximize}} \left| \sum_{c=1}^{N_C} v_{\text{BL},c}^* x_c \right|^2, \text{ s.t. } |x_c|^2 \leq P_{\max}, \forall c, \quad (39)$$

where $v_{\text{BL},c}$ is the c -th element of \mathbf{v}_{BL} , and the objective function is maximized for

$$x_c = \sqrt{P_{\max}} \frac{v_{\text{BL},c}}{|v_{\text{BL},c}|} = \sqrt{P_{\max}} e^{j\theta} \frac{h_{C,c}^*}{|h_{C,c}|}, \quad (40)$$

where $h_{C,c}$ and x_c are the c -th element of \mathbf{h}_C and the optimal BF vector $\mathbf{x}_{\text{BF}'}$, respectively.

C. Beamforming Design for \mathcal{P}_{DLI} and $\mathcal{P}'_{\text{DLI}}$

Using the equality $\|\mathbf{A}\|^2 = \text{Tr}\{\mathbf{A}\mathbf{A}^H\}$ and the cyclic property of the trace operator, the problem \mathcal{P}_{DLI} for the given set \mathcal{S} can be written as

$$\begin{aligned} \mathcal{P}_{\text{DLI},1} : & \underset{\mathbf{x} \in \mathbb{C}^{N_C \times 1}}{\text{maximize}} && \text{Tr}\{\mathbf{H}_{\text{BL}}^H \mathbf{H}_{\text{BL}} \mathbf{x} \mathbf{x}^H\} \\ & \text{s.t.} && \frac{\text{Tr}\{\mathbf{h}_{\text{DL},r}^* \mathbf{h}_{\text{DL},r}^T \mathbf{x} \mathbf{x}^H\}}{\text{Tr}\{\mathbf{h}_{\text{BL},r}^* \mathbf{h}_{\text{BL},r}^T \mathbf{x} \mathbf{x}^H\}} \leq \alpha, \forall r/r_{\text{ref}}, \\ & && \text{Tr}\{\mathbf{x} \mathbf{x}^H\} \leq P_{\max}. \end{aligned} \quad (41)$$

The solution is obtained through two steps as described below.

1) Step 1 - Semidefinite Relaxation

Let us define $\mathbf{G}_{\text{BL}} = \mathbf{H}_{\text{BL}}^H \mathbf{H}_{\text{BL}}$, $\mathbf{G}_{\text{BL}}^r = \mathbf{h}_{\text{BL},r}^* \mathbf{h}_{\text{BL},r}^T$, $\mathbf{G}_{\text{DL}}^r = \mathbf{h}_{\text{DL},r}^* \mathbf{h}_{\text{DL},r}^T$, and $\mathbf{X} = \mathbf{x}\mathbf{x}^H$. Then, the problem in (41) is

$$\begin{aligned} & \underset{\mathbf{X} \in \mathbb{C}^{N_C \times N_C}}{\text{maximize}} && \text{Tr}\{\mathbf{G}_{\text{BL}}\mathbf{X}\} \\ & \text{s.t.} && \text{Tr}\{(\mathbf{G}_{\text{DL}}^r - \alpha \mathbf{G}_{\text{BL}}^r)\mathbf{X}\} \leq 0, \forall r/r_{\text{ref}}, \\ & && \text{Tr}\{\mathbf{X}\} \leq P_{\text{max}}, \mathbf{X} \succeq 0, \text{rank}(\mathbf{X}) = 1. \end{aligned} \quad (42)$$

The problem in (42) is a non-convex optimization problem due to the constraint $\text{rank}(\mathbf{X}) = 1$. Thus, we can apply semidefinite relaxation (SDR) by dropping the rank-1 constraint to convert the problem into a convex optimization problem, \mathcal{P}_{SDR} , with a globally optimal solution.

2) Step 2 - Optimization Toolbox for the Solution

The problem \mathcal{P}_{SDR} can be solved using the interior point method and convex optimization toolbox (CVX). The global optimal solution of the problem \mathcal{P}_{SDR} is denoted as \mathbf{X}_{opt} .

The best rank-1 approximation of \mathbf{X}_{opt} is given by $\lambda_{\text{opt}} \mathbf{q}_{\text{opt}} \mathbf{q}_{\text{opt}}^H$, where $\lambda_{\text{opt}} \in \mathbb{C}$ is the largest eigenvalue of \mathbf{X}_{opt} , and $\mathbf{q}_{\text{opt}} \in \mathbb{C}^{N_C \times 1}$ is the corresponding eigenvector and $\|\mathbf{q}_{\text{opt}}\| = 1$ [41]. Then, the solution to the problem $\mathcal{P}_{\text{DLI},1}$ is the scaled version of the dominant eigenvector of \mathbf{X}_{opt} given by

$$\mathbf{x}_{\text{DLI}} = \sqrt{P_{\text{max}}} \mathbf{q}_{\text{opt}}. \quad (43)$$

BF design for $\mathcal{P}'_{\text{DLI}}$: For the scenario with per antenna constraint, $\mathcal{P}'_{\text{DLI}}$ with the given set \mathcal{S} , we can also follow the aforementioned steps. Thus, the relaxed problem for $\mathcal{P}'_{\text{DLI}}$ can be defined by just replacing the constraint $\text{Tr}\{\mathbf{X}\} \leq P_{\text{max}}$ in (42) by $[\mathbf{X}]_{c,c} \leq P_{\text{max}}, \forall c$, which limits the transmitted energy per transmit antenna. The solution for $\mathcal{P}'_{\text{DLI}}$ is called $\mathbf{x}_{\text{DLI}'}$ which can be calculated similar to (43).

D. Beamforming Design for $\mathcal{P}_{\alpha 0}$

The problem $\mathcal{P}_{\alpha 0}$ for the given set \mathcal{S} can be written as

$$\mathcal{P}_{\alpha 0,1} : \underset{\mathbf{x} \in \mathbb{C}^{N_C \times 1}}{\text{maximize}} \quad \|\mathbf{H}_{\text{BL}}\mathbf{x}\|^2, \text{ s.t. (30b), } \mathbf{x} \in N(\mathbf{H}'_{\text{DL}}). \quad (44)$$

The orthonormal basis for the nullspace of \mathbf{H}'_{DL} is created using the $N_C - r_{\text{DL}}$ right singular vectors of \mathbf{H}'_{DL} corresponding to its zero singular values. This basis is denoted by $\mathbf{Z}_{\text{DL}} \in \mathbb{C}^{N_C \times N_C - r_{\text{DL}}}$ where $\mathbf{Z}_{\text{DL}}^H \mathbf{Z}_{\text{DL}} = \mathbf{I}_{N_C - r_{\text{DL}}}$ and $r_{\text{DL}} = \text{rank}(\mathbf{H}'_{\text{DL}}) \leq \min\{N_R - M_{\text{ref}}, N_C\}$. In $\mathcal{P}_{\alpha 0,1}$, the vector \mathbf{x} can be written as $\mathbf{x} = \mathbf{Z}_{\text{DL}}\mathbf{b}$, where $\mathbf{b} \in \mathbb{C}^{N_C - r_{\text{DL}} \times 1}$, to remove the constraint $\mathbf{x} \in N(\mathbf{H}'_{\text{DL}})$ as

$$\underset{\mathbf{b}}{\text{maximize}} \quad \|\mathbf{H}_{\text{BL}}\mathbf{Z}_{\text{DL}}\mathbf{b}\|^2, \text{ s.t. } \|\mathbf{Z}_{\text{DL}}\mathbf{b}\|^2 = \|\mathbf{b}\|^2 \leq P_{\text{max}}. \quad (45)$$

Similar to the solution of (36), the solution for the above problem is the right singular vector of $\mathbf{H}_{\text{BL}}\mathbf{Z}_{\text{DL}}$. Thus, the optimal solution for the problem in (45) is $\mathbf{b}_{\text{opt}} = \sqrt{P_{\text{max}}} \mathbf{v}_{\text{Z}}$, where $\mathbf{v}_{\text{Z}} \in \mathbb{C}^{N_C - r_{\text{DL}} \times 1}$ is the right singular vector. Then, the optimal solution for $\mathcal{P}_{\alpha 0,1}$ is

$$\mathbf{x}_{\alpha 0} = \sqrt{P_{\text{max}}} \mathbf{Z}_{\text{DL}} \mathbf{v}_{\text{Z}}, \quad (46)$$

which lies in the nullspace of \mathbf{H}'_{DL} because $\mathbf{x}_{\alpha 0}$ is the combination of the columns of \mathbf{Z}_{DL} . Note that the optimal solution

can be rewritten as

$$\mathbf{x}_{\alpha 0} = \sqrt{P_{\text{max}}} e^{j\theta} \mathbf{Z}_{\text{DL}} \mathbf{Z}_{\text{DL}}^H \mathbf{h}_C^* / \|\mathbf{Z}_{\text{DL}} \mathbf{h}_C^*\|, \exists \theta \in \mathbb{R}, \quad (47)$$

where $\mathbf{Z}_{\text{DL}} \mathbf{Z}_{\text{DL}}^H$ is a projection matrix to the nullspace of \mathbf{H}'_{DL} . The optimal BF vector in (47) is the scaled version of the projection of (37) to the nullspace of \mathbf{H}'_{DL} .

E. Beamforming Design for $\mathcal{P}'_{\alpha 0}$

The problem $\mathcal{P}'_{\alpha 0}$ for the given set \mathcal{S} can be written as

$$\begin{aligned} \mathcal{P}'_{\alpha 0,1} : & \underset{\mathbf{x} \in \mathbb{C}^{N_C \times 1}}{\text{maximize}} \quad \|\mathbf{H}_{\text{BL}}\mathbf{x}\|^2 \\ & \text{s.t.} \quad \mathbf{H}'_{\text{DL}}\mathbf{x} = 0, |x_c|^2 \leq P_{\text{max}}, \forall c. \end{aligned} \quad (48)$$

This is a non-convex problem due to the maximization of the norm. Using the SVD of \mathbf{H}_{BL} , the objective function can be reformulated as $|\mathbf{v}_{\text{BL}}^H \mathbf{x} e^{j\theta}|^2$, where θ is an arbitrary phase rotation. Without loss of optimality, θ can be chosen such that the objective becomes a real-valued quantity, i.e., $|\mathbf{v}_{\text{BL}}^H \mathbf{x} e^{j\theta}| = \text{Re}\{\mathbf{v}_{\text{BL}}^H \mathbf{x}\}$. Therefore, the problem can be equivalently rewritten as

$$\begin{aligned} & \underset{\mathbf{x} \in \mathbb{C}^{N_C \times 1}}{\text{maximize}} \quad \text{Re}\{\mathbf{v}_{\text{BL}}^H \mathbf{x}\} \\ & \text{s.t.} \quad \mathbf{H}'_{\text{DL}}\mathbf{x} = 0, |x_c|^2 \leq P_{\text{max}}, \forall c. \end{aligned} \quad (49)$$

Note that this reformulated problem is convex and equivalent to $\mathcal{P}'_{\alpha 0,1}$, and can be efficiently solved using standard convex optimization solvers.

Closed form BF design for $\mathcal{P}'_{\alpha 0,1}$: We relax the constraint $|x_c|^2 \leq P_{\text{max}}$ in (48) to $\|\mathbf{x}\|^2 \leq P_{\text{max}}$. With this relaxation, the solution is the same with (46). Due to the original constraint $|x_c|^2 \leq P_{\text{max}}$, we scale the solution, and the final sub-optimal closed-form solution can be given as

$$\mathbf{x}_{\alpha 0'} = \sqrt{P_{\text{max}}} \mathbf{Z}_{\text{DL}} \mathbf{v}_{\text{Z}} / q_{\text{max}}, \quad (50)$$

where q_{max} represents the maximum absolute value among the elements of $\mathbf{Z}_{\text{DL}} \mathbf{v}_{\text{Z}}$.

F. Beamforming Design for $\mathcal{P}_{\text{multi}}$

We use a bisection method to solve $\mathcal{P}_{\text{multi}}$. The overall bisection method is summarized in Algorithm 3.

We first define $\mathbf{x} = \mathbf{Z}_{\text{DL}}\mathbf{b}$ as in $\mathcal{P}_{\alpha 0}$. For the given set \mathcal{S} , the problem $\mathcal{P}_{\text{multi}}$ is equivalent to

$$\begin{aligned} & \underset{\mathbf{b}}{\text{maximize}} \quad t \\ & \text{s.t.} \quad \text{SINR}_k \geq t, \forall k, \\ & \quad \|\mathbf{b}\|^2 \leq P_{\text{max}}, \end{aligned} \quad (51)$$

where $t = \min_k \text{SINR}_k$. For a given t , we check feasibility via the following problem:

$$\begin{aligned} & \text{find } \mathbf{b} \\ & \text{s.t.} \quad \text{SINR}_k \geq t, \forall k, \\ & \quad \|\mathbf{b}\|^2 \leq P_{\text{max}}. \end{aligned} \quad (52)$$

We define the following matrices

$$\begin{aligned} \mathbf{A}_k &= \delta_k \left\| \mathbf{h}_R^k \right\|^4 \mathbf{Z}_{\text{DL}}^H (\mathbf{h}_C^k)^* (\mathbf{h}_C^k)^T \mathbf{Z}_{\text{DL}}, \\ \mathbf{B}_k &= \mathbf{Z}_{\text{DL}}^H \mathbf{H}_{\text{DL}}^H \mathbf{h}_R^k (\mathbf{h}_R^k)^H \mathbf{H}_{\text{DL}} \mathbf{Z}_{\text{DL}}, \\ \mathbf{C}_k &= \mathbf{Z}_{\text{DL}}^H \sum_{k' \neq k} \left(\delta_{k'} (\mathbf{H}_{\text{BL}}^{k'})^H \mathbf{h}_R^k (\mathbf{h}_R^k)^H \mathbf{H}_{\text{BL}}^{k'} \right) \mathbf{Z}_{\text{DL}}. \end{aligned}$$

Algorithm 3 Bisection Algorithm for $\mathcal{P}_{\text{multi}}$

Input: $\mathbf{A}_k, \mathbf{B}_k, \mathbf{C}_k$ for all k , P_{max} , \mathbf{Z}_{DL} , and ϵ

- 1: **Initialize:** Initialize the bisection bounds: t_{\min} and t_{\max} .
- 2: **while** $t_{\max} - t_{\min} > \epsilon$ **do**
- 3: Set $t \leftarrow \frac{t_{\min} + t_{\max}}{2}$
- 4: Solve the feasibility problem in (52).
- 5: **if** the problem is feasible **then**
- 6: Update lower bound: $t_{\min} \leftarrow t$
- 7: Update beamforming vector: \mathbf{b}^*
- 8: **else**
- 9: Update upper bound: $t_{\max} \leftarrow t$
- 10: **end if**
- 11: **end while**

Output: The beamforming vector $\mathbf{Z}_{\text{DL}} \mathbf{b}^*$

Using these matrices, the SINR constraint for the k -th BD is

$$\mathbf{b}^H (\mathbf{A}_k - t(\mathbf{B}_k + \mathbf{C}_k)) \mathbf{b} \geq \|\mathbf{h}_R^k\|^2 t, \quad \forall k. \quad (53)$$

The feasibility problem in (52) is solved by applying semidefinite relaxation as in Section VI-C.

VII. PROPOSED AP PARTITIONING ALGORITHMS

In this section, we propose algorithms for AP role selection for all problems outlined in Table II, using the BF vectors derived in Section VI. The problem \mathcal{P}_{BF} is solved using dynamic programming (DP). The remaining problems are solved using an iterative optimization algorithm.

A. AP Partitioning Algorithm for \mathcal{P}_{BF}

When we substitute the optimal BF vector \mathbf{x}_{BF} given in (37) to \mathcal{P}_{BF} given in (30), the constraint $\|\mathbf{x}\|^2 \leq P_{\text{max}}$ holds with equality and \mathcal{P}_{BF} is reduced solely to the AP role selection, and it can be expressed as

$$\underset{\mathcal{S}}{\text{maximize}} \quad \|\mathbf{h}_R\|^2 \|\mathbf{h}_C\|^2, \quad \text{s.t. } \mathbf{AP}_{\text{ref}} \in \mathcal{S}_R. \quad (54)$$

To maximize the objective function in (54), $\|\mathbf{h}_R\|^2$ and $\|\mathbf{h}_C\|^2$ should ideally be equal to $\sum_{l \in \mathcal{L}} \|\mathbf{h}_l\|^2 / 2$. As a result, the problem in (54) is equivalent to

$$\underset{\mathcal{S}_\kappa}{\text{maximize}} \quad \sum_{l \in \mathcal{S}_\kappa} \|\mathbf{h}_l\|^2, \quad \text{s.t. } \sum_{l \in \mathcal{S}_\kappa} \|\mathbf{h}_l\|^2 \leq \sum_{l \in \mathcal{L}} \|\mathbf{h}_l\|^2 / 2, \quad (55)$$

where \mathcal{S}_κ ($\kappa \in \{CE, R\}$) is a subset of \mathcal{L} . If the solution set includes \mathbf{AP}_{ref} , $\kappa = R$ and \mathcal{S}_κ gives the set of readers, otherwise $\kappa = CE$. This problem is similar to the subset sum problem, a special case of the Knapsack problem, and can be solved using a greedy algorithm or DP [42].

Unlike greedy algorithms, DP generally converges to optimal solutions. In DP, integers are generally used, thus we reformulate the problem in (55) by rounding the floats to integers. Let us define integer weights $q_l = \lfloor s \|\mathbf{h}_l\|^2 + 0.5 \rfloor$, where s is a scaling factor affecting the precision. Then, the relaxed problem can be formulated as

$$\underset{\mathcal{S}_\kappa}{\text{maximize}} \quad \sum_{l \in \mathcal{S}_\kappa} q_l, \quad \text{s.t. } \sum_{l \in \mathcal{S}_\kappa} q_l \leq \left\lfloor \sum_{l \in \mathcal{L}} \frac{1}{2} q_l \right\rfloor = Q. \quad (56)$$

Algorithm 4 DP for AP Partitioning

Input: \mathcal{L}, q_k, Q

Output: \mathcal{S}_κ

- 1: $OP(0, q) = 0, \forall q$
- 2: **for** $l' \leftarrow 1$ to L **do**
- 3: **for** $q \leftarrow 0$ to Q **do**
- 4: **if** $q_{l'} > q$ **then**
- 5: $OP(l', q) = OP(l' - 1, q)$
- 6: Save the AP indices maximizing $OP(l', q)$.
- 7: **else**
- 8: $OP(l', q) = \max(OP(l' - 1, q),$
 $q_{l'} + OP(l' - 1, q - q_{l'}))$
- 9: Save the AP indices maximizing $OP(l', q)$.
- 10: **end if**
- 11: **end for**
- 12: **end for**

For this case, DP provides the optimal solution. However, the optimal solution for (56) may not be optimal for (55) due to the rounding errors and low precision. With the increasing scaling factor, the optimal solutions for (56) and (55) will approach each other at the cost of increasing the algorithm's complexity.

The DP algorithm creates small subproblems and recursively solves these subproblems to reach the final solution. In total, we have $L(Q+1)$ subproblems, one for each element of \mathcal{L} and $q \in \{0, 1, \dots, Q\}$. Let us define a subproblem for parameters l' and q as follows

$$\mathcal{P}_{l', q} : \underset{\mathcal{S}_{l'}}{\text{maximize}} \quad \sum_{l \in \mathcal{S}_{l'}} q_l, \quad \text{s.t. } \sum_{l \in \mathcal{S}_{l'}} q_l \leq q, \quad (57)$$

where $\mathcal{S}_{l'} \subseteq \{1, 2, \dots, l'\}$ is a subset of first l' AP, and $OP(l', q)$ denotes the optimal maximum value of the subproblem $\mathcal{P}_{l', q}$. The initial values are $OP(0, q) = 0, \forall q$. Then, we solve the subproblems recursively using the following rule [42]

$$OP(l', q) = \begin{cases} OP(l' - 1, q) & \text{if } q < q_{l'}, \\ \max(OP(l' - 1, q), q_{l'} + OP(l' - 1, q - q_{l'})) & \text{otherwise.} \end{cases} \quad (58)$$

The summary of the algorithm is given in Algorithm 4. For example, if the weight for $\mathbf{AP}_{l'}$ exceeds the summation constraint q , then $\mathcal{P}_{l', q}$ and $\mathcal{P}_{l'-1, q}$ have identical solutions, so $OP(l', q) = OP(l' - 1, q)$. Conversely, if the weight of $\mathbf{AP}_{l'}$ is at most q , we use the optimal solution calculated previously for $\mathcal{P}_{l'-1, q-q_{l'}}$, aiming to maximize the objective function using the subset of the first $l' - 1$ APs with a constraint $q - q_{l'}$. Then, the solution to $\mathcal{P}_{l', q}$ is determined by taking the greater value between $OP(l' - 1, q)$ and $q_{l'} + OP(l' - 1, q - q_{l'})$. This approach reduces complexity by calculating $OP(l', q)$ from $OP(l' - 1, q)$ and $OP(l' - 1, q - q_{l'})$, achieving a time complexity of $\mathcal{O}(LQ)$, in contrast to the exponential complexity of $\mathcal{O}(2^L)$ for an exhaustive search. More details on DP can be found in [42].

When computing each $OP(l', q)$ value, we store the APs indices. Finally, the APs indices for $OP(L, Q)$ are the set of selected CEs if \mathbf{AP}_{ref} is included; otherwise, they correspond

to the readers for the problem in (56). In summary, for the problem \mathcal{P}_{BF} , the solution of $OP(L, Q)$ is the CEs (or readers) while the remaining APs are readers (or CEs).

B. AP Partitioning Algorithm for the Remaining Problems

In this subsection, we give the details of the proposed AP role selection algorithm for all problems except \mathcal{P}_{BF} . Searching for all possible combinations of CEs and readers is not a feasible solution because the computational complexity of the exhaustive search increases with increasing number of APs. Thus, the proposed algorithm uses a coalitional game theory approach to find the set of CEs and readers among the given APs.

1) Coalition Game

In this cooperative game, the set of APs \mathcal{L} are cooperative players that form coalitions. We have two coalitions, sets of CEs (\mathcal{S}_{CE}) and readers (\mathcal{S}_{R}), and the partition of the given APs are defined as $\mathcal{S} = \{\mathcal{S}_{\text{CE}}, \mathcal{S}_{\text{R}}\}$. The union of these two sets includes all APs while the intersection of them is empty as $\mathcal{L} = \mathcal{S}_{\text{CE}} \cup \mathcal{S}_{\text{R}}$ and $\mathcal{S}_{\text{CE}} \cap \mathcal{S}_{\text{R}} = \emptyset$.

The non-transferable utility function is defined as $U(\mathcal{S}) = \|\mathbf{H}_{\text{BL}}\mathbf{x}\|^2$. In addition, we define the function $C(\mathcal{S}) = \max_{r/r_{\text{ref}}} \left(\left| \mathbf{h}_{\text{DL},r}^T \mathbf{x} \right|^2 / \left| \mathbf{h}_{\text{BL},r}^T \mathbf{x} \right|^2 \right)$, which is used to check whether the constraint on DLI is satisfied for each reader antenna except the AP_{ref} antennas. Note that, $U(\mathcal{S}) = t$ and $C(\mathcal{S}) = \max_{k,r/r_{\text{ref}}} \left(\left| (\mathbf{h}_{\text{DL},r}^k)^T \mathbf{x} \right|^2 / \left| (\mathbf{h}_{\text{BL},r}^k)^T \mathbf{x} \right|^2 \right)$ for $\mathcal{P}_{\text{multi}}$. If the reader set only includes AP_{ref} , then $C(\mathcal{S}) = 0$. The role of an AP depends on the increase/decrease in the utility function and the DLI constraint. After the initial partition, AP_l will switch its role based on the following operations:

- **Switch Operation:** Let us define \mathcal{S}_{κ} as the set of readers (CEs) and $\mathcal{S}_{\kappa'}$ as the set of CEs (readers) where $\kappa, \kappa' \in \{\text{CE}, \text{R}\}$. The preference relation $\mathcal{S}' \succ_l \mathcal{S}$ implies that AP_l in \mathcal{S}_{κ} prefers to be a member of $\mathcal{S}_{\kappa'}$, where \mathcal{S}' is the new set of CEs and readers and defined as $\mathcal{S}' = \{\mathcal{S}_{\kappa} \setminus \{l\}, \mathcal{S}_{\kappa'} \cup \{l\}\}$. This rule can be written as

$$\mathcal{S}' \succ_l \mathcal{S} \Leftrightarrow U(\mathcal{S}_{\kappa} \setminus \{l\}, \mathcal{S}_{\kappa'} \cup \{l\}) > U(\mathcal{S}), C(\mathcal{S}') \leq \alpha, \quad (59)$$

where $l \in \mathcal{L}/\text{ref}$. If there is no DLI constraint, we do not check $C(\mathcal{S}') \leq \alpha$ for switch operation.

- **Swap Operation:** The swap operation is defined as follows

$$\mathcal{S} = \{\mathcal{S}_{\kappa}, \mathcal{S}_{\kappa'}\} \rightarrow \mathcal{S}' = \{\mathcal{S}_{\kappa} \setminus \{l\} \cup \{l'\}, \mathcal{S}_{\kappa'} \setminus \{l'\} \cup \{l\}\}, \quad (60)$$

where $l, l' \in \mathcal{L}/\text{ref}$, and AP_l swaps its coalition with $\text{AP}_{l'}$ if $U(\mathcal{S}') > U(\mathcal{S})$ and $C(\mathcal{S}') \leq \alpha$. When there is no DLI constraint, we only check whether $U(\mathcal{S}') > U(\mathcal{S})$.

Note that for $\mathcal{P}_{\text{multi}}$, neither the switch nor the swap operation is performed if the problem in (52) is infeasible for the given CE and reader sets.

2) Proposed Solution Based on Coalition Game Algorithm

The proposed algorithm consists of four phases:

Phase 1 - Initial Set of CEs and Readers: In \mathcal{P}'_{BF} , there is no DLI constraint. Therefore, we randomly select APs as CEs and readers and use this initial set as input for Algorithm 5. However, we always put the AP_{ref} to the reader set.

Algorithm 5 Coalitional Game Algorithm

Input: $\mathcal{L}, \mathcal{S}_{\text{init}}, \text{AP}_{\text{ref}}, \alpha, P_{\text{max}}, \mathbf{H}_{\text{BL}}, \mathbf{H}_{\text{DL}}, \mathbf{H}'_{\text{DL}}$

Output: \mathcal{S}, \mathbf{x}

```

1:  $\mathcal{S} \leftarrow \mathcal{S}_{\text{init}}$ 
2: while convergence = 0 do ▷ We have the solution if
   convergence is 1.
3:    $\mathcal{L}_{\text{aux}} \leftarrow \mathcal{L}/\text{AP}_{\text{ref}}$ 
4:    $\mathcal{S}_{\text{prev}} \leftarrow \mathcal{S}$ 
5:   while  $|\mathcal{L}_{\text{aux}}| \neq 0$  do ▷ We iterate over all APs.
6:     Select a random AP,  $\text{AP}_l$ , from the set  $\mathcal{L}_{\text{aux}}$ .
7:     if  $|\mathcal{S}_{\kappa}| \neq 1$  then
8:        $\mathcal{S}_{\text{aux}} \leftarrow \{\mathcal{S}_{\kappa} \setminus \{l\}, \mathcal{S}_{\kappa'} \cup \{l\}\}$ .
9:       Calculate  $U(\mathcal{S}_{\text{aux}}), C(\mathcal{S}_{\text{aux}})$  and BF vector using
the
       results in Section VI.
10:      if  $\mathcal{S}_{\text{aux}} \succ_l \mathcal{S}$  then
11:         $\mathcal{S} \leftarrow \mathcal{S}_{\text{aux}}$ 
12:         $\mathbf{x} \leftarrow \mathbf{x}_{\text{aux}}$ 
13:      end if
14:    end if
15:    Delete the  $\text{AP}_l$  from the set  $\mathcal{L}_{\text{aux}}$ 
16:  end while
17:  if  $\mathcal{S} = \mathcal{S}_{\text{prev}}$  then
18:    convergence = 1.
19:  end if
20: end while

```

For the remaining problems, which have DLI constraint, we randomly select an initial set of CEs and readers ($\mathcal{S}_{\text{init}}$), ensuring AP_{ref} is in the reader set. Then we verify the DLI constraint, i.e., $C(\mathcal{S}_{\text{init}}) \leq \alpha$. If it is satisfied, the initial set is provided as input to Algorithm 5. Otherwise, we generate new sets at random until the constraint is met or the number of generated initial sets reaches a predefined threshold, i.e., ζ_{init} . If the number of initial sets reaches ζ_{init} , the final set is used as input for Algorithm 5, and $U(\mathcal{S}_{\text{init}})$ is set to zero if $C(\mathcal{S}_{\text{init}}) > \alpha$.

Phase 2 - Algorithm 5: In this phase, Algorithm 5 iterates over all APs except AP_{ref} , performing the following steps in each iteration:

- **Step 1:** An AP is selected randomly.
- **Step 2:** If feasible, a switch operation changes the AP's role.
- **Step 3:** The BF vector is recalculated.
- **Step 4:** If the switch operation improves the utility function and meets the DLI constraint (if applicable), the updated CEs and readers set are retained; otherwise, they revert to the original configuration.

The steps above are repeated until convergence is achieved. In Algorithm 5, let us assume AP_l is randomly selected in Step 1. Then, \mathcal{S}_{κ} represents the set containing AP_l , while $\mathcal{S}_{\kappa'}$ denotes the complementary set. If AP_l is part of the CE set, then $\mathcal{S}_{\kappa} = \mathcal{S}_{\text{CE}}$ and $\mathcal{S}_{\kappa'} = \mathcal{S}_{\text{R}}$. If $|\mathcal{S}_{\kappa}| = 1$ when AP_l is selected, the switch operation cannot be applied, and \mathcal{S} remains unchanged.

Phase 3 - DLI Constraint: Since the number of possible

Algorithm 6 Swap Algorithm**Input:** $\mathcal{S}, \mathbf{x}, \text{AP}_{\text{ref}}, \alpha, P_{\text{max}}, \mathbf{H}_{\text{BL}}, \mathbf{H}_{\text{DL}}$ **Output:** \mathcal{S}, \mathbf{x}

```

1: Calculate  $U(\mathcal{S}) = \|\mathbf{H}_{\text{BL}}\mathbf{x}\|^2$ .
2: for  $l \leftarrow 1$  to  $|\mathcal{S}_{\text{CE}}|$  do
3:   for  $l' \leftarrow 1$  to  $|\mathcal{S}_{\text{R}}|$  do
4:      $\mathcal{S}_{\text{aux}} = \{\mathcal{S}_{\text{CE}} \setminus \{\mathcal{S}_{\text{CE}}(l)\} \cup \{\mathcal{S}_{\text{R}}(l')\},$ 
        $\mathcal{S}_{\text{R}} \setminus \{\mathcal{S}_{\text{R}}(l')\} \cup \{\mathcal{S}_{\text{CE}}(l)\}\}$ 
       (If  $\mathcal{S}_{\text{R}}(l') = \text{ref}$ , skip the loop for this particular  $l'$ .)
5:     Calculate the BF vector  $\mathbf{x}_{\text{aux}}, U(\mathcal{S}_{\text{aux}})$ , and  $C(\mathcal{S}_{\text{aux}})$ .
6:     if  $U(\mathcal{S}_{\text{aux}}) > U(\mathcal{S})$  and  $C(\mathcal{S}_{\text{aux}}) \leq \alpha$  (if applicable)
       then
7:        $\mathcal{S} \leftarrow \mathcal{S}_{\text{aux}}$ 
8:        $\mathbf{x} \leftarrow \mathbf{x}_{\text{aux}}$ 
9:     end if
10:  end for
11: end for

```

AP partitions is finite, and each switch operation strictly increases the utility function as shown in (59), Algorithm 5 is guaranteed to converge to a set \mathcal{S}^* where no feasible switch operation can result in a higher utility. This can be expressed as $U(\mathcal{S}^*) \geq U(\mathcal{S})$, where \mathcal{S}^* is the output of Algorithm 5 and no further improvement is possible through any feasible switch operation that leads to a new partition \mathcal{S} . After the convergence, Algorithm 5 provides the set of CEs and readers.

If the initial set from Phase 1 does not satisfy the DLI constraint, the output set from Algorithm 5 may not satisfy $C(\mathcal{S}) \leq \alpha$. If that is the case, Phase 1 and 2 are repeated until either $C(\mathcal{S}) \leq \alpha$ is satisfied after Phase 2 or a predetermined threshold for the maximum number of repetitions of the first two phases, i.e., ζ_{Alg5} , is reached.

For \mathcal{P}'_{BF} , Phase 1 and 2 are repeated ζ_{Alg5} times with different initial solutions since there is no DLI constraint. Then, the best solution is selected.

Phase 4 - Algorithm 6: Once Phase 3 is completed, the set \mathcal{S} is provided as input to Algorithm 6 which swaps each element of the CE set with each element of the reader set except AP_{ref} . If the utility function improves and DLI constraint (if present) is satisfied after the swap operation, the changes are kept. The result of Algorithm 6 is the final set of CEs and readers.

C. Greedy AP Partitioning Algorithm

In this subsection, a simpler iterative AP selection algorithm is introduced for all the problems. Initially, AP_{ref} is selected as a reader, and a randomly selected AP is assigned as a CE. In each iteration, one AP is randomly selected and assigned to the set that yields a higher objective, i.e., $\|\mathbf{H}_{\text{BL}}\mathbf{x}\|^2$ or t , while the DLI constraint is satisfied ($C(\mathcal{S}) \leq \alpha$). If the constraint is not satisfied, the AP remains unassigned. The process continues until all APs are evaluated. This algorithm offers a lightweight alternative for the AP selection.

VIII. COMPLEXITY ANALYSIS

This section provides a computational complexity analysis of the proposed algorithms.

Channel Estimation: For notational simplicity, we assume that $M_l = M$ and $\tau_{p,l} = \tau_p$ for all $l \in \mathcal{L} \setminus \text{ref}$. The complexity of line 1 in Algorithm 2 is $\mathcal{O}(J'M_{\text{ref}}\tau_{p,\text{ref}} + M_{\text{ref}}^2\tau_{p,\text{ref}} + M_{\text{ref}}^3)$. The complexity of line 6 is $\mathcal{O}(\zeta_{\text{chn}}T(J'M_{\text{ref}}^2 + (L-1)J'MM_{\text{ref}}))$. The complexity of line 7 is $\mathcal{O}(\zeta_{\text{chn}}(L-1)(M_{\text{ref}}M + J'M_{\text{ref}}\tau_p + M_{\text{ref}}^2\tau_p + M_{\text{ref}}^3))$. The complexity of line 10 is $\mathcal{O}(\zeta_{\text{chn}}(L-1)J'M\tau_p + \zeta_{\text{chn}}LJ'M_{\text{ref}}\tau_p)$. The overall complexity is the summation of the given complexities above. For $M_{\text{ref}} = 1$, the overall complexity reduces to $\mathcal{O}(J'\tau_{p,\text{ref}} + (L-1)(M + J'\tau_p))$, offering a more efficient implementation and reduced hardware cost due to fewer high-resolution ADCs. For the multiple BD case, Algorithm 2 is executed for each BD.

Proposed BF Designs: The problems $\mathcal{P}_{\text{BF}}, \mathcal{P}'_{\text{BF}}$, and $\mathcal{P}_{\alpha 0}$, given in Section VI, have low complexities due to the closed-form solutions. Their worst-case complexity is approximately $\mathcal{O}(\max(N_{\text{C}}, N_{\text{R}}) \min(N_{\text{C}}, N_{\text{R}})^2)$, which corresponds to the cost of computing SVD. For $\mathcal{P}'_{\alpha 0}$ in (49), the complexity is $\mathcal{O}(N_{\text{C}}^{3.5})$ [43]. For the remaining problems using semidefinite programming (SDP) the complexity is $\mathcal{O}(\sqrt{a} \log(1/\epsilon)(ba^3 + b^2a^2 + b^3))$, where $a \times a$ is the size of the positive semidefinite matrix, b is the number of constraints, and ϵ is the solution accuracy [44]. For example, the complexity of solving the problem in (42) is approximately $\mathcal{O}(\sqrt{N_{\text{C}}} \log(1/\epsilon)(N_{\text{R}}N_{\text{C}}^3 + N_{\text{R}}^2N_{\text{C}}^2 + N_{\text{R}}^3))$. The complexity of Algorithm 3 is $\mathcal{O}(\log(1/\epsilon)B)$, where ϵ is the accuracy in bisection method, and B is the complexity of solving the SDP problem in (52).

AP Partitioning Algorithms: As mentioned earlier, the complexity of DP is $\mathcal{O}(LQ)$. In Algorithm 5, the primary computational cost arises from the BF vector calculation. Therefore, the complexity of Algorithm 5 is approximately $\mathcal{O}(I_{\text{out}}LB)$, where I_{out} is the number of outer loop iterations until convergence, and B is the complexity of the BF design. In practice, I_{out} is typically small, keeping the overall complexity moderate despite the algorithm's iterative nature. Similarly, in Algorithm 6, the BF vector computation is the dominant cost, leading to an overall complexity of approximately $\mathcal{O}(|\mathcal{S}_{\text{CE}}||\mathcal{S}_{\text{R}}|B)$. The complexity of the greedy AP partitioning algorithm is $\mathcal{O}(LB)$.

IX. NUMERICAL RESULTS

This section presents the simulation parameters and results. We use the following parameters: $\lambda = 0.1$ m, $J = 1$, $\gamma_j^0 = -1$, $\gamma_j^1 = 1$ and the vertical and horizontal inter antenna distances are 0.5λ for APs. The term λ stands for the wavelength of the emitted signal. The solutions of the optimization problems, except for $\mathcal{P}_{\text{multi}}$, do not depend on P_{max} . Therefore, we select $P_{\text{max}} = 1$ to solve these problems. Unless otherwise stated, there are 11 APs ($L = 11$), and the first 10 AP have 4×4 antennas in x - z axis, i.e., $M_l = 16$, $l \in \mathcal{L} \setminus \text{ref}$. However, AP_{11} is the reference AP equipped with a single antenna ($M_{11} = 1$) and 16-bit ADC. This choice of $M_{11} = 1$ aims to achieve a system that is cost-effective and power-efficient. While the reference AP is located at (10, 5, 2) meters (m), the remaining APs are distributed horizontally on the two

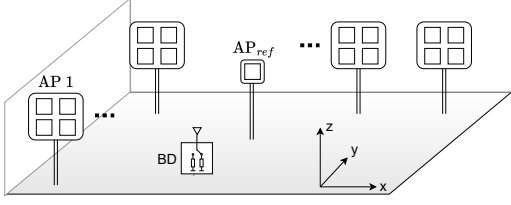


Fig. 2: All APs and BD are located indoors with six reflectors: the side walls, the ground, and the ceiling.

TABLE III: Summary of the Results for the Setup in Fig. 3a

Problem	BF Vector	PG at BD	$\ \mathbf{H}_{\text{BL}}\mathbf{x}\ ^2$	$C(\mathcal{S}_{\text{final}})$
\mathcal{P}_{BF}	(37)	-36.0 dB	-72.1 dB	58.2 dB
\mathcal{P}_{DLI}	(43) (CVX)	-34.9 dB	-73.5 dB	0 dB
$\mathcal{P}_{\alpha 0}$	(46)	-35 dB	-73.6 dB	-261.5 dB
\mathcal{P}'_{BF}	(40)	-36.2 dB	-52.2 dB	48.7 dB
$\mathcal{P}'_{\text{DLI}}$	Section VI-C	-36 dB	-54.8 dB	0 dB
$\mathcal{P}'_{\alpha 0}$	Section VI-E	-36.2 dB	-55 dB	-190.3 dB
	(50)	-36.1 dB	-58.1 dB	-257.1 dB

sides of the environment at $y = 1$ m and $y = 9$ m. The center of each AP is located at $z = 2$ m. Unless otherwise stated, there is a single BD located at $(4, 4, 2)$ m. The simulation environment is illustrated in Fig. 2, which considers a room of $20 \times 10 \times 4$ m with six reflectors: four side walls, ground, and ceiling.

The channels are modeled as ⁴

$$\begin{aligned}
 [\mathbf{H}_{\text{DL}}]_{r,c} &= \frac{\lambda}{4\pi d_{r,c}} e^{-j\frac{2\pi}{\lambda} d_{r,c}} + \sum_{m=1}^5 \frac{g_{\text{SMC}} \lambda}{4\pi d_{r,c}^m} e^{-j\frac{2\pi}{\lambda} d_{r,c}^m}, \\
 h_{\text{C},c} &= \frac{\lambda}{4\pi d_c} e^{-j\frac{2\pi}{\lambda} d_c} + \sum_{m=1}^5 \frac{g_{\text{SMC}} \lambda}{4\pi d_c^m} e^{-j\frac{2\pi}{\lambda} d_c^m}.
 \end{aligned} \quad (61)$$

The distances $d_{r,c}$ and d_c stand for the free-space line-of-sight (LoS) path lengths between the c -th antenna in the CE set and r -th antenna in the reader set, and c -th antenna in the CE set and the BD antenna, respectively. The distances $d_{r,c}^m$ and d_c^m stands for the non-LoS path lengths due to the first-order reflections. The channel $h_{\text{R},r}$ is defined similar to $h_{\text{C},c}$, but using the distances between r -th antenna in the reader set and the BD antenna, i.e., d_r and d_r^m . The amplitude gain of the specular multipath components (SMCs) generated by specular reflections are $g_{\text{SMC}} = 0.5$.

Given that the elements of the noise vector have unit variance, the received SNR is defined as $\text{SNR} = P_{\text{max}} \bar{\beta}^2$, where $\bar{\beta}$ is the average path loss between an antenna of an AP and the BD. During the channel estimation phase, SNR is denoted as SNR_p . The term $\bar{\beta} = -53.4$ dB is found by Monte-Carlo simulations for randomly distributed BD.

Table III presents some of the optimization problems and the corresponding equation numbers to design the BF vectors. While (37), (40), (46), and (50) are the closed-form low-complexity solutions, the remaining solutions are obtained by solving the problems in CVX. For the AP partitioning, we use

⁴Note that given the narrowband nature of BC and the larger coherence bandwidth of the channel, we assume a frequency-flat channel model, despite the presence of multipath components.

the DP method with $s = 10^8$ introduced in Section VII-A for \mathcal{P}_{BF} . For all other problems, unless stated otherwise, we use the algorithm described in Section VII-B. For the closed-form solutions, we set $\zeta_{\text{init}} = 30$ and $\zeta_{\text{Alg5}} = 4$. For the CVX implementations, both parameters are set to 1, except for $\mathcal{P}_{\text{multi}}$, where we set $\zeta_{\text{init}} = 30$ and $\zeta_{\text{Alg5}} = 4$.

For \mathcal{P}_{DLI} and $\mathcal{P}'_{\text{DLI}}$, while $\alpha = 0$ dB when solving the optimization problems, we use $\alpha = 0 + \epsilon$ dB only for comparison purposes, $C(\mathcal{S}) \leq 0 + \epsilon$ dB, where ϵ is a small positive number. For $\mathcal{P}_{\alpha 0}$, $\mathcal{P}'_{\alpha 0}$, and $\mathcal{P}_{\text{multi}}$ while $\alpha = -\infty$ dB when solving the optimization problems, we use $\alpha = -100$ dB for comparison purposes, $C(\mathcal{S}) \leq -100$ dB. Note that the problem \mathcal{P}_{BF} , which uses MRT as a BF technique, and \mathcal{P}'_{BF} will serve as benchmark methods.

The path gain, PG, represents the ratio of the received energy to the transmitted energy, calculated by

$$\text{PG} = \left| \mathbf{h}_{\text{C}}^T \mathbf{x} \right|^2 / \|\mathbf{x}\|^2, \quad (62)$$

where \mathbf{h}_{C} shows the channel between CEs and the location where PG is calculated.

A. PG and P_e Analyses for a Fixed Setup with Perfect CSI

In this subsection, all problems are analyzed for fixed AP and BD locations with perfect CSI. The results are summarized in Table III, where $\mathcal{S}_{\text{final}}$ is the final set of CEs and readers.

Furthermore, all the results in Table III obtained using the proposed algorithms match the optimal solutions found through exhaustive search by checking all possible CE and reader sets combinations. While the optimality of the proposed algorithms cannot be proven, they achieve the optimal performance for the evaluated specific scenarios.

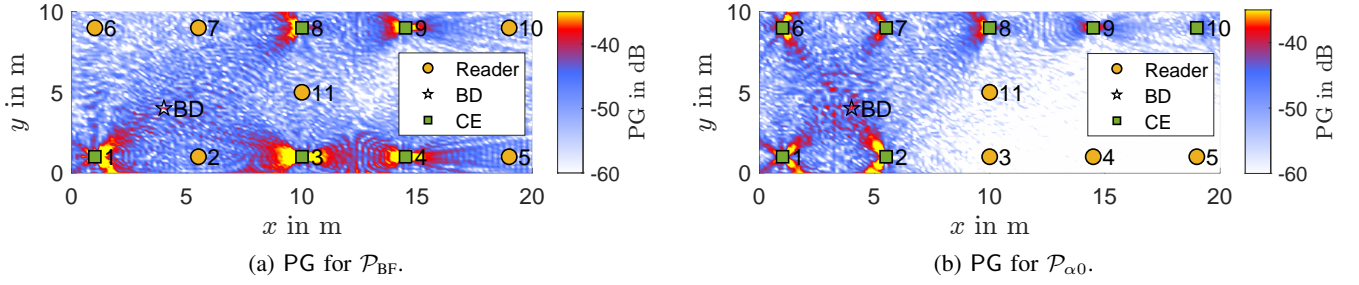
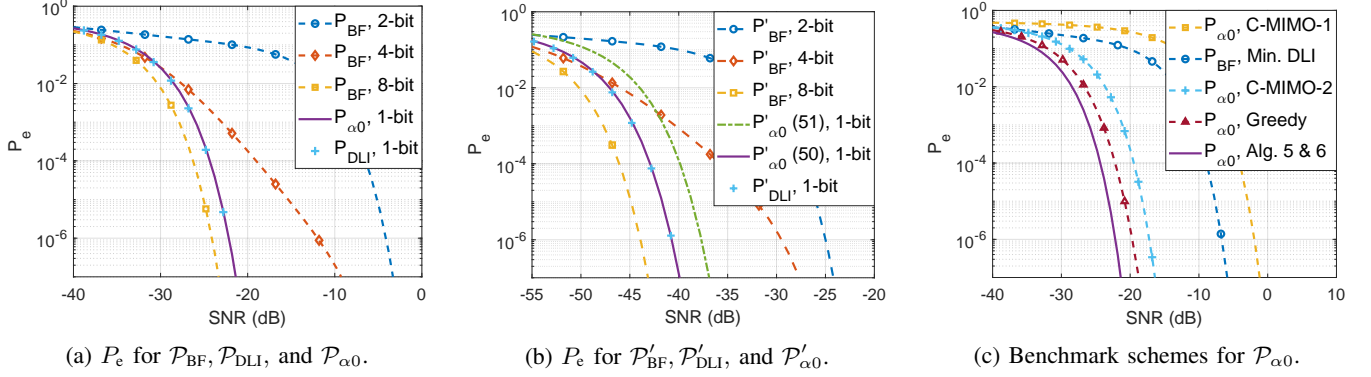
1) Path Gain Analyses for \mathcal{P}_{BF} and $\mathcal{P}_{\alpha 0}$

Figs. 3a and 3b show the path gains at $z = 2$ m for the problems \mathcal{P}_{BF} and $\mathcal{P}_{\alpha 0}$, respectively. In Fig. 3a, while the energy is focused on the BD location, the readers are exposed to the DLI ($C(\mathcal{S}_{\text{final}}) = 48.32$ dB) decreasing the performance. In contrast, $\mathcal{P}_{\alpha 0}$ mitigates DLI by considering it in the AP role selection and BF design, as shown in Fig. 3b, where $C(\mathcal{S}_{\text{final}}) = -259.24$ dB and energy is focused on the BD. This allows readers to receive the backscattered signal without interference, significantly improving performance in terms of P_e . Note that there is no need to cancel the interference in the location of AP₁₁, which has high resolution ADC.

2) P_e Analysis for \mathcal{P}_{BF} , $\mathcal{P}_{\alpha 0}$, \mathcal{P}_{DLI}

In Fig. 4a, we compare the P_e performance of \mathcal{P}_{BF} , $\mathcal{P}_{\alpha 0}$, and \mathcal{P}_{DLI} with $\alpha = 1$ for the given AP and BD locations. We use (24) to calculate P_e . For the \mathcal{P}_{BF} case, for a higher b than $b = 8$, the improvement in P_e will be negligible. In addition, \mathcal{P}_{BF} with $b = 2$ has the worst performance due to the quantization errors.

In the CVX solution of \mathcal{P}_{DLI} , the final set of CEs and readers from $\mathcal{P}_{\alpha 0}$ is used as an initial set. As shown in the figure, the performance of \mathcal{P}_{DLI} is nearly identical to the performance of $\mathcal{P}_{\alpha 0}$. This is because, as seen in Table III, the increase in the objective function in \mathcal{P}_{DLI} relative to $\mathcal{P}_{\alpha 0}$ is insufficient to produce a noticeable performance gain for the given scenario.

Fig. 3: PG at $z = 2$ m for $M_l = 16, M_{11} = 1$.Fig. 4: Comparison of P_e performance under different setups with perfect CSI.

The proposed method $\mathcal{P}_{\alpha 0}$ with $b = 1$ outperforms \mathcal{P}_{BF} with $b = 2$ and $b = 4$ due to DLI cancellation and closely matches the performance of \mathcal{P}_{BF} with $b = 8$. Therefore, $\mathcal{P}_{\alpha 0}$ is the preferred solution for the DLI cancellation due to its simplicity and optimal closed-form BF design.

3) P_e Analysis for $\mathcal{P}'_{BF}, \mathcal{P}'_{\alpha 0}, \mathcal{P}'_{DLI}$

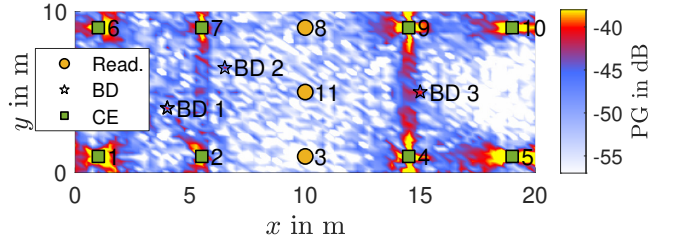
In Fig. 4b, we compare the P_e performance of $\mathcal{P}'_{BF}, \mathcal{P}'_{\alpha 0}$, and \mathcal{P}'_{DLI} with $\alpha = 1$. For the same error probability, there is an approximate 3 dB SNR gap between $\mathcal{P}'_{BF}, b = 8$ case and $\mathcal{P}'_{\alpha 0}(49), b = 1$ case solved using CVX. Despite this, the slopes of the P_e curves are nearly identical. Therefore, the proposed method $\mathcal{P}'_{\alpha 0}$ with $b = 1$ can achieve the same error probability as $\mathcal{P}'_{BF}, b = 8$ by increasing the transmit power, eliminating the need for power-hungry high-resolution ADCs.

Note that the final set of CEs and readers obtained from solving $\mathcal{P}'_{\alpha 0}$ using (50) are used as the initial set for the CVX solutions of $\mathcal{P}'_{\alpha 0}$ and \mathcal{P}'_{DLI} , and the performance gap between closed-form ((50)) and CVX solutions of $\mathcal{P}'_{\alpha 0}$ is around 3 dB. Although the CVX solution performs better, the closed-form solution offers significantly lower complexity, making it more efficient for fast-varying channel conditions.

In addition, the performances of \mathcal{P}'_{DLI} and $\mathcal{P}'_{\alpha 0}(49)$ are nearly identical because a slight increase in the objective function of \mathcal{P}'_{DLI} compared to $\mathcal{P}'_{\alpha 0}$ does not lead to a noticeable performance improvement, as seen in Table III.

4) Additional Benchmark Schemes

Fig. 4c illustrates the P_e calculated as in (24) for different benchmark schemes, namely $\mathcal{P}_{\alpha 0}$ with C-MIMO-1, C-MIMO-2, and greedy, and \mathcal{P}_{BF} with minimum DLI.

Fig. 5: PG for \mathcal{P}_{multi} .

For the \mathcal{P}_{BF} case, we set $b = 2$, design \mathbf{x} using (38), and select the AP partitioning via exhaustive search to minimize the DLI, resulting in $C(\mathcal{S}) = 37.8$ dB. In all other scenarios, we set $b = 1$. For $\mathcal{P}_{\alpha 0}$, greedy and $\mathcal{P}_{\alpha 0}$, Alg. 5 & 6 scenarios, we use the AP partitioning algorithm given in Section VII-C and VII-B, respectively.

In C-MIMO-1 and C-MIMO-2 cases, there is a single CE and a single reader, with their centers located at coordinates (1, 5, 2) and (19, 5, 2) m, respectively. In the C-MIMO-1 scenario, both the CE and the reader are equipped with 9×9 antennas, while in the C-MIMO-2 scenario, the CE has 12×12 antennas and the reader has 4×4 antennas. For a fair comparison, one of the reader's antennas is equipped with a high-resolution ADC in both cases. C-MIMO-2 achieves better performance than C-MIMO-1 due to its larger number of degrees of freedom, resulting from a higher-dimensional null space of \mathbf{H}'_{DL} .

In addition, the proposed $\mathcal{P}_{\alpha 0}$ scheme using Algorithms 5 and 6 has the best performance compared to all the benchmarks. The $\mathcal{P}_{\alpha 0}$, greedy case provides a near-optimal solution and

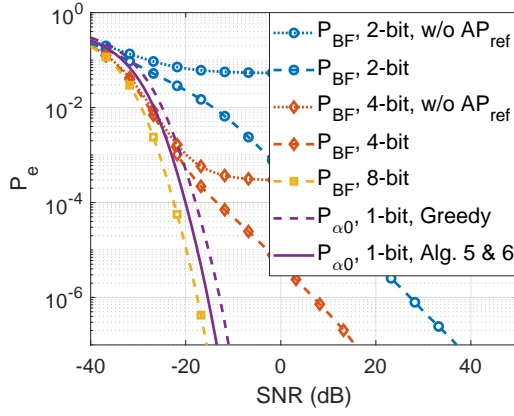


Fig. 6: P_e for \mathcal{P}_{BF} and $\mathcal{P}_{\alpha 0}$ with/without AP_{ref} .

offers a more computationally efficient alternative.

5) PG Analyses for the Multiple BDs Case

In this case, there are three BDs, denoted as BD 1, BD 2, and BD 3, located at (4, 4, 2), (6.5, 6.5, 2), and (15, 5, 2) m, respectively. The SNR is set to 10 dB, and $\delta_k = 1$.

We investigate two different scenarios. In Scenario 1, it is assumed that BDs use orthogonal reflection coefficients. Accordingly, we set $\mathbf{B}_k = 0$ and $\mathbf{C}_k = 0$ in (53) when solving the BF design problem. As a result, the problem \mathcal{P}_{multi} reduces to maximizing $\min_k \|\mathbf{H}_{BL}^k \mathbf{x}\|^2$, subject to the transmit power and DLI constraints. Fig. 5 shows the resulting path gains at $z = 2$ m. As shown in the figure, the DLI around the readers is mitigated ($C(S_{final}) = -243$ dB), and energy is concentrated on the BDs, and $\|\mathbf{H}_{BL}^k \mathbf{x}\|^2 / \|\mathbf{x}\|^2 = -78.3$ dB, $\forall k$.

In Scenario 2, we compute \mathbf{B}_k and \mathbf{C}_k , and consider them in (53) while maximizing the minimum SINR across all BD. As a result, $\text{SINR}_k = 22.7$ dB, $\|\mathbf{H}_{BL}^k \mathbf{x}\|^2 / \|\mathbf{x}\|^2 \approx -80 \pm 1$ dB, $\forall k$, and $C(S_{final}) = -245$ dB. In summary, the proposed algorithms are also effective in scenarios with multiple BDs, achieving balanced SINR_k while satisfying the DLI constraint.

B. Comparison of P_e for Random Setups with Perfect CSI

In Fig. 6, P_e is calculated using (24) under perfect CSI for different numbers of bits in the ADCs using Monte-Carlo simulations. We analyze the cases with and without AP_{ref} . For without AP_{ref} case, AP_{ref} has the same number of ADC bits as the other APs and is treated as a regular AP, eliminating the need to include it in the reader set. CSI can be estimated without AP_{ref} using geometric methods if the propagation environment, the locations of the APs and BD are known [45]. For this reason, we present the results where AP_{ref} is a regular AP.

For each realization, there is a single BD and its coordinate is uniformly distributed as $\mathcal{U}(0, 20)$, $\mathcal{U}(0, 10)$, and $\mathcal{U}(0, 2)$ along the x , y , and z axes, respectively, while the APs positions remain fixed.

In Fig. 6, \mathcal{P}_{BF} with $b = 2$ and $b = 4$ w/o AP_{ref} show the performance when AP_{ref} is treated as a regular AP. The performances of \mathcal{P}_{BF} , $b = 8$ and $\mathcal{P}_{\alpha 0}$ without AP_{ref} are not given because the performances with and without AP_{ref} are

almost identical.

In Fig. 6, the error floors in \mathcal{P}_{BF} with $b = 4$ and $b = 2$ without AP_{ref} are due to DLI and quantization noise. The proposed method, $\mathcal{P}_{\alpha 0}$ with $b = 1$, eliminates the error floor with 1-bit ADCs, and significantly outperforms \mathcal{P}_{BF} with $b = 2$ and $b = 4$. Although \mathcal{P}_{BF} with $b = 8$ slightly outperforms $\mathcal{P}_{\alpha 0}$ with Algorithms 5 and 6, the proposed method achieves the same performance as \mathcal{P}_{BF} with $b = 8$ by increasing the SNR by approximately 2.5 dB relative to \mathcal{P}_{BF} , thereby eliminating the need for high-resolution ADCs. In summary, the proposed method not only improves P_e but also reduces the required ADC resolution compared to \mathcal{P}_{BF} .

In addition, $\mathcal{P}_{\alpha 0}$ using Algorithms 5 and 6 achieves approximately a 2 dB SNR improvement over the greedy approach. While the greedy algorithm has a slightly lower performance, it provides a solution with reduced computational complexity.

C. P_e Analyses for a Fixed Setup with Imperfect CSI

In this subsection, all problems are analyzed for fixed APs and the single BD locations with imperfect CSI. While \mathbf{H}_{DL} is perfectly known, all \mathbf{h}_l s are estimated using the method in Section III. P_e , calculated using (28), is averaged over different estimations.

Since AP_{ref} has a single antenna, no iteration is required during channel estimation. The parameter J' is set to $J' = 2$; however, as an exception, it is increased to $J' = 8$ during the estimation of \mathbf{h}_{ref} . In Figs. 7 and 8, the solid lines represent the performance under perfect CSI, while the dashed lines show the performance under imperfect CSI.

In Fig. 7, $\text{SNR}_p = 6$ dB, and poor channel estimation causes an error floor in \mathcal{P}_{BF} , $b = 8$. At high SNR, \mathcal{P}_{BF} , $b = 2$ outperforms \mathcal{P}_{BF} , $b = 8$ because, in the case of \mathcal{P}_{BF} , $b = 2$, the diagonal element of $\hat{\mathbf{D}}_j^{-1}$ corresponding to AP_{ref} dominates over the other diagonal elements due to the significant ADC bit difference between AP_{ref} and the remaining APs, as shown in (17). Thus, the detector primarily relies on AP_{ref} 's signal, with minimal loss from the combination of signals from other readers.

In Fig. 7, a phenomenon similar to that of the \mathcal{P}_{BF} , $b = 2$ case at high SNR values is also observed for $\mathcal{P}_{\alpha 0}$. While $\mathcal{P}_{\alpha 0}$ outperforms \mathcal{P}_{BF} with $b = 2$ at low SNR values, it performs worse than \mathcal{P}_{BF} with $b = 2$ at high SNR values, primarily due to the nullspace constraint combined with the limitations of poor channel estimation quality. In addition, $\mathcal{P}_{\alpha 0}$ offers better performance compared to the \mathcal{P}_{BF} , $b = 8$ case at high SNR values. In summary, when channel estimation quality is inadequate for coherent operations of APs, it is more advantageous to rely solely on the received signal from a single antenna at high SNR values. This approach eliminates the need for signal combining at the readers, thereby reducing the impact of estimation errors and ensuring more robust performance in such scenarios.

In Fig. 8, $\text{SNR}_p = 10$ dB, and the results for perfect and imperfect CSI are highly similar, indicating that the channel estimates are sufficient for the coherent operation of APs. Interestingly, the performance of \mathcal{P}_{BF} , $b = 2$ under imperfect CSI is slightly better than that of perfect CSI in the low SNR region due to the difference in AP role selection affecting the

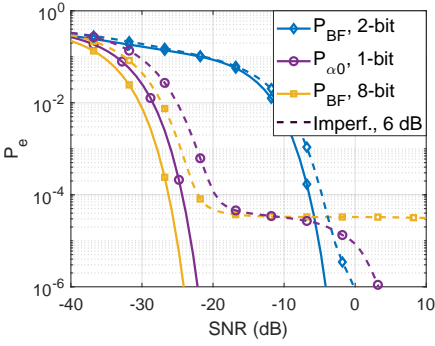


Fig. 7: P_e for \mathcal{P}_{BF} and $\mathcal{P}_{\alpha 0}$ under imperfect CSI when $\text{SNR}_p = 6$ dB.

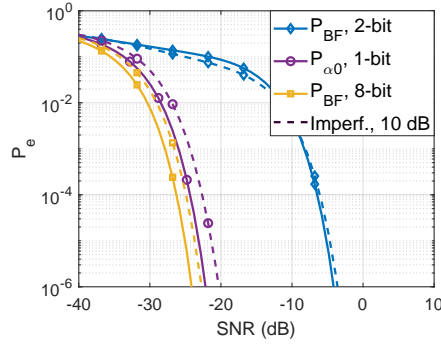


Fig. 8: P_e for \mathcal{P}_{BF} and $\mathcal{P}_{\alpha 0}$ under imperfect CSI when $\text{SNR}_p = 10$ dB.

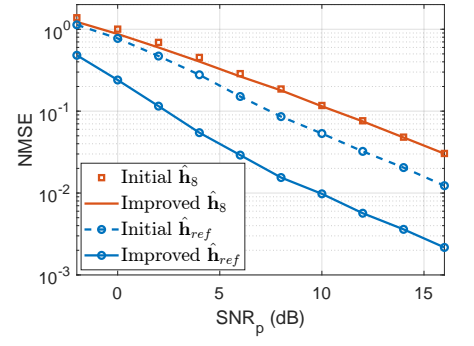


Fig. 9: NMSE with and without iteration in the channel estimation.

DLI. In summary, the proposed $\mathcal{P}_{\alpha 0}$ method offers the cost- and energy-efficient solution, leveraging the use of 1-bit ADC.

D. Performance Analyses for the Proposed Channel Estimation Algorithm

This subsection evaluates the proposed channel estimation algorithm with fixed APs and BD locations. AP_{ref} has a 2×2 antenna array ($M_{11} = 4$) along the x - z plane, and J' is set to 1. In Algorithm 1, the learning rate $\alpha_{lr} = 100$ and maximum iteration $T = 100$, and $\zeta_{\text{chn}} = 4$ in Algorithm 2.

In Fig. 9, we compare the normalized mean square error (NMSE) for \mathbf{h}_l with and without iterations in the channel estimation algorithm for different SNR_p values. For the non-iterative case, the initial estimates of \mathbf{h}_{ref} from Step 1 and \mathbf{h}_l from Step 2 are used.

The NMSE is defined as

$$\text{NMSE} = \mathbb{E} \left\{ \left\| \mathbf{h}_l - e^{j\theta} \hat{\mathbf{h}}_l \right\|^2 / \left\| \mathbf{h}_l \right\|^2 \right\}, \quad (63)$$

where the expectation is taken over $\hat{\mathbf{h}}_l$. Note that all $\hat{\mathbf{h}}_l$ s are exposed to the same phase change due to the phase ambiguity in $\hat{\mathbf{h}}_{\text{ref}}$. However, this does not impact the design of the transmitted vector \mathbf{x} , as explained in Section III-B. Consequently, $e^{j\theta}$, where $\theta \in \{0, \pi\}$, is used to eliminate the effect of the phase ambiguity due to the estimate of \mathbf{h}_{ref} .

In Fig. 9, NMSE is calculated by Monte-Carlo simulations. The performance of the estimation algorithm with iteration is slightly better than that without iteration for $\hat{\mathbf{h}}_s$ at low SNR values. At high SNR values, the estimates of \mathbf{h}_s with and without iterations become nearly identical. The results for other $\hat{\mathbf{h}}_l$ values are omitted because they exhibit similar behavior to $\hat{\mathbf{h}}_s$. However, the proposed channel estimation algorithm significantly decreases NMSE for $\hat{\mathbf{h}}_{\text{ref}}$ across all SNR values.

X. CONCLUSION

In this paper, we address the critical challenges of DLI and round-trip path loss in BiBC systems operating in distributed MIMO setups. The proposed joint AP selection and novel BF strategies enhance the received backscattered energy and effectively mitigate DLI, resulting in reduced error probabilities.

A tailored channel estimation algorithm is developed to tackle the impact of DLI, along with theoretical derivations for

the probability of error for BC under both perfect and imperfect CSI. The proposed iterative channel estimation algorithm improves the estimation quality compared to the initial estimates. Furthermore, the quantization noise caused by DLI is modeled to provide practical insights into system performance.

Simulation results show that the proposed problems ($\mathcal{P}_{\text{DLI}}, \mathcal{P}'_{\text{DLI}}, \mathcal{P}_{\alpha 0}, \mathcal{P}'_{\alpha 0}, \mathcal{P}_{\text{multi}}$) and algorithms effectively focus energy on the BD and cancel DLI, thereby minimizing quantization noise. Using energy-efficient 1-bit ADCs, the proposed methods achieve performance comparable to benchmark setups ($\mathcal{P}_{\text{BF}}, \mathcal{P}'_{\text{BF}}$) employing higher-resolution ADCs. Consequently, the proposed methods deliver an energy- and cost-efficient solution for BC in multiple-antenna systems by eliminating the need for power-hungry ADCs while maintaining high performance.

APPENDIX

In this appendix⁵, we present the formulation and solution of an alternative optimization problem, which maximizes $\left\| \mathbf{D}^{-1/2} \mathbf{H}_{\text{BL}} \mathbf{x} \right\|^2$ instead of $\left\| \mathbf{H}_{\text{BL}} \mathbf{x} \right\|^2$.

We can maximize $\left\| \mathbf{D}^{-1/2} \mathbf{H}_{\text{BL}} \mathbf{x} \right\|^2$ under a *total* power constraint, resulting in the problem⁶

$$\begin{aligned} \mathcal{P}_D : \quad & \underset{\mathbf{x} \in \mathbb{C}^{N_C \times 1}, \mathcal{S}}{\text{maximize}} \quad \left\| \mathbf{D}^{-1/2} \mathbf{H}_{\text{BL}} \mathbf{x} \right\|^2 \\ \text{s.t.} \quad & \left\| \mathbf{x} \right\|^2 \leq P_{\text{max}}, \text{AP}_{\text{ref}} \in \mathcal{S}_R. \end{aligned} \quad (64)$$

Alternatively, we can maximize $\left\| \mathbf{D}^{-1/2} \mathbf{H}_{\text{BL}} \mathbf{x} \right\|^2$ under *per-antenna* power constraints, resulting in

$$\begin{aligned} \mathcal{P}'_D : \quad & \underset{\mathbf{x} \in \mathbb{C}^{N_C \times 1}, \mathcal{S}}{\text{maximize}} \quad \left\| \mathbf{D}^{-1/2} \mathbf{H}_{\text{BL}} \mathbf{x} \right\|^2 \\ \text{s.t.} \quad & |x_c|^2 \leq P_{\text{max}}, \text{AP}_{\text{ref}} \in \mathcal{S}_R. \end{aligned} \quad (65)$$

for $c = 1, \dots, N_C$.

Details and solutions of the new problems \mathcal{P}_D and \mathcal{P}'_D are given below.

⁵Note that the appendix in this arXiv version is provided as the supplementary material of the IEEE version of the paper.

⁶For simplicity, the index j in \mathbf{D} is omitted because all reflection coefficients have the same magnitude and thus \mathbf{D} is independent of j .

A. Total Power Constraint (\mathcal{P}_D)

For the given AP partitioning, the problem is

$$\mathcal{P}_{D,1} : \underset{\mathbf{x} \in \mathbb{C}^{N_C \times 1}}{\text{maximize}} \quad \left\| \mathbf{D}^{-1/2} \mathbf{H}_{BL} \mathbf{x} \right\|^2, \quad \text{s.t.} \quad \|\mathbf{x}\|^2 \leq P_{\max}, \quad (66)$$

where \mathbf{D} is a function of \mathbf{x} .

We employ the quadratic transform developed in [38] (for a different problem with the same structure). The problem $\mathcal{P}_{D,1}$ is equivalent to

$$\underset{\mathbf{x} \in \mathbb{C}^{N_C \times 1}, \mathbf{z} \in \mathbb{C}^{N_R \times 1}}{\text{maximize}} \quad 2 \operatorname{Re} \{ \mathbf{z}^H \mathbf{H}_{BL} \mathbf{x} \} - \mathbf{z}^H \mathbf{D} \mathbf{z}, \quad \text{s.t.} \quad \|\mathbf{x}\|^2 \leq P_{\max}. \quad (67)$$

We solve the problem by alternating optimization (AO), where \mathbf{x} and \mathbf{z} are optimized in turn until convergence. For given \mathbf{x} , the optimal \mathbf{z} is [38]

$$\mathbf{z} = \mathbf{D}^{-1} \mathbf{H}_{BL} \mathbf{x}. \quad (68)$$

For given \mathbf{z} , dropping the constant terms in the objective function in (67), the problem can be reformulated as

$$\mathcal{P}_{D,\mathbf{x}} : \underset{\mathbf{x} \in \mathbb{C}^{N_C \times 1}}{\text{minimize}} \quad \mathbf{x}^H \mathbf{A} \mathbf{x} - 2 \operatorname{Re} \{ \mathbf{z}^H \mathbf{H}_{BL} \mathbf{x} \}, \quad \text{s.t.} \quad \|\mathbf{x}\|^2 \leq P_{\max}, \quad (69)$$

where

$$\mathbf{A} = \sum_{r=1}^{N_r} |z_r|^2 \frac{\mathbf{h}_{DL,r}^* \mathbf{h}_{DL,r}^T + \delta \mathbf{h}_{BL,r}^* \mathbf{h}_{BL,r}^T}{2^{2b_r} \times 3} \succeq 0, \quad (70)$$

for the given channel coefficients and z_r is the r -th element of \mathbf{z} . Problem (69) is convex and satisfies Slater's condition (e.g., $\mathbf{x} = 0$ is strictly feasible), so the Karush–Kuhn–Tucker (KKT) conditions are necessary and sufficient for optimality. The KKT conditions for (69) yield the solution as

$$\mathbf{x} = (\mathbf{A} + \mu \mathbf{I})^{-1} \mathbf{H}_{BL}^H \mathbf{z}, \quad \mu \geq 0, \quad (71)$$

where the Lagrange multiplier μ is chosen as follows: if the unconstrained solution $\mathbf{x} = \mathbf{A}^{-1} \mathbf{H}_{BL}^H \mathbf{z}$ satisfies $\|\mathbf{x}\|^2 \leq P_{\max}$, then $\mu = 0$; otherwise, μ is selected (e.g., by a bisection search) such that $\|\mathbf{x}\|^2 = P_{\max}$.

B. Per-Antenna Power Constraint (\mathcal{P}'_D)

The problem with the per-antenna transmit power constraint, for a given AP partitioning, is

$$\mathcal{P}'_{D,1} : \underset{\mathbf{x} \in \mathbb{C}^{N_C \times 1}}{\text{maximize}} \quad \left\| \mathbf{D}^{-1/2} \mathbf{H}_{BL} \mathbf{x} \right\|^2, \quad \text{s.t.} \quad |x_c|^2 \leq P_{\max}, \forall c. \quad (72)$$

After the quadratic transform, similar to (67), the problem can be expressed as

$$\underset{\mathbf{x} \in \mathbb{C}^{N_C \times 1}, \mathbf{z} \in \mathbb{C}^{N_R \times 1}}{\text{maximize}} \quad 2 \operatorname{Re} \{ \mathbf{z}^H \mathbf{H}_{BL} \mathbf{x} \} - \mathbf{z}^H \mathbf{D} \mathbf{z}, \quad \text{s.t.} \quad |x_c|^2 \leq P_{\max}. \quad (73)$$

The solution for \mathbf{z} given in Eq. (68) still holds. For the given \mathbf{z} , the problem is convex and given as

$$\mathcal{P}'_{D,\mathbf{x}} : \underset{\mathbf{x} \in \mathbb{C}^{N_C \times 1}}{\text{minimize}} \quad \mathbf{x}^H \mathbf{A} \mathbf{x} - 2 \operatorname{Re} \{ \mathbf{z}^H \mathbf{H}_{BL} \mathbf{x} \}, \quad \text{s.t.} \quad |x_c|^2 \leq P_{\max}, \quad (74)$$

where the optimal \mathbf{x} can be found by projected gradient descent (PGD). The details are as follows.

PGD update: Let $g(\mathbf{x}) = \mathbf{A}^T \mathbf{x}^* - \mathbf{H}_{BL}^T \mathbf{z}^*$ be the gradient of the objective in (74) with respect to (w.r.t.) \mathbf{x} [33]. The objective is L_A -smooth with Lipschitz constant $L_A = 2\lambda_{\max}(\mathbf{A})$, where

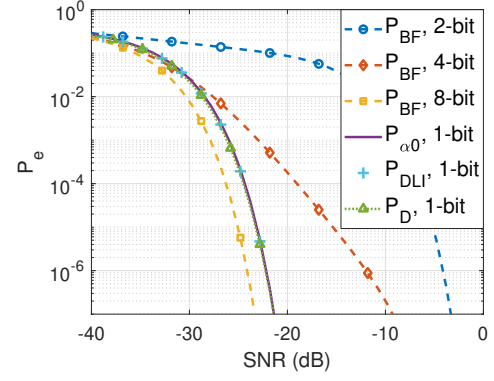


Fig. 10: P_e for \mathcal{P}_{BF} , \mathcal{P}_{DLI} , $\mathcal{P}_{\alpha 0}$, and \mathcal{P}_D .

$\lambda_{\max}(\mathbf{A})$ is the maximum eigenvalue of \mathbf{A} . With a step size $\eta \in (0, 1/L_A]$, the PGD updates are given by

$$\mathbf{x}^{(t+1)} = \Pi_{\mathcal{C}} \left(\mathbf{x}^{(t)} - \eta \left(g(\mathbf{x}^{(t)}) \right)^* \right), \quad (75)$$

where $\mathcal{C} = \{\mathbf{x} : |x_c|^2 \leq P_{\max}\}$ is the feasible set, and $\Pi_{\mathcal{C}}(\cdot)$ denotes the projection onto \mathcal{C} . Since the constraint is separable across elements of \mathbf{x} , the projection is performed element-wise as

$$[\Pi_{\mathcal{C}}(\mathbf{x})]_c = \begin{cases} x_c, & |x_c| \leq \sqrt{P_{\max}}, \\ \sqrt{P_{\max}} \frac{x_c}{|x_c|}, & |x_c| > \sqrt{P_{\max}}. \end{cases} \quad (76)$$

For convex and L_A -smooth objectives, PGD with $\eta \in (0, 1/L_A]$ is guaranteed to converge to the global minimizer of the problem.

An algorithm outline for both $\mathcal{P}_{D,1}$ and $\mathcal{P}'_{D,1}$ is given below:

- 1) Initialize \mathbf{x} (pick any feasible point).
- 2) Repeat until convergence:
 - a) $\mathbf{z} \leftarrow \mathbf{D}^{-1} \mathbf{H}_{BL} \mathbf{x}$.
 - b) For $\mathcal{P}_{D,\mathbf{x}}$: $\mathbf{x} \leftarrow (\mathbf{A} + \mu \mathbf{I})^{-1} \mathbf{H}_{BL}^H \mathbf{z}$ with $\mu \geq 0$.
 - For $\mathcal{P}'_{D,\mathbf{x}}$: $\mathbf{x} \leftarrow \text{PGD}$.

C. Complexity Analysis

This section provides a computational complexity analysis of \mathcal{P}_D and \mathcal{P}'_D for the BF design.

In both problems, the AO framework iteratively updates \mathbf{x} and the auxiliary variable \mathbf{z} . For each AO iteration, the complexity of \mathcal{P}_D is approximately $\mathcal{O}(N_R N_C^2 + N_C^3)$, while the complexity of \mathcal{P}'_D is $\mathcal{O}(N_R N_C^2 + \frac{L_A}{\epsilon} N_C^2)$. Here, $\mathcal{O}(L_A/\epsilon)$ denotes the number of PGD iterations required to achieve an ϵ -accurate solution.

D. Numerical Results

We compare the probability of error performance of the original problems $\mathcal{P}_{\alpha 0}$ and $\mathcal{P}'_{\alpha 0}$ with that of the new problems \mathcal{P}_D and \mathcal{P}'_D . We assume the fixed setup with perfect CSI.

For AP selection in \mathcal{P}_D and \mathcal{P}'_D , we employ Algorithm 5 and Algorithm 6. As in \mathcal{P}'_{BF} , there is no DLI constraint for the new problems \mathcal{P}_D and \mathcal{P}'_D . Therefore, we randomly select APs as CEs and readers and use this initial set as input for Algorithm 5. In Algorithm 5, Phases 1 and 2 are repeated ζ_{Alg5} times with different initial solutions. Then, the best solution is selected.

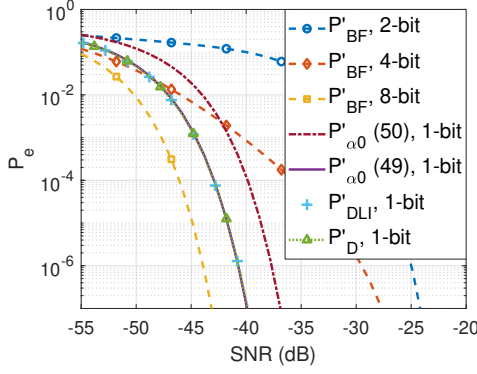


Fig. 11: P_e for \mathcal{P}'_{BF} , \mathcal{P}'_{DLI} , $\mathcal{P}'_{\alpha0}$, and \mathcal{P}'_D .

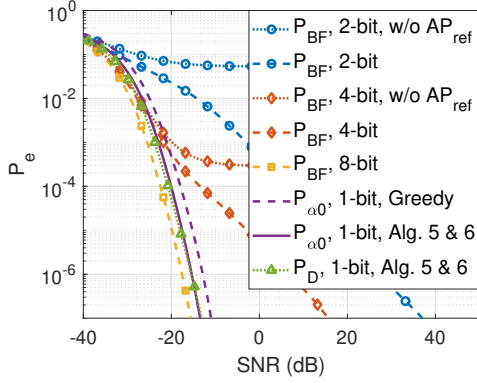


Fig. 12: P_e for \mathcal{P}_{BF} , $\mathcal{P}_{\alpha0}$, and \mathcal{P}_D .

Figs. 10 and 11 compare the results for \mathcal{P}_D and \mathcal{P}'_D , with the results from Figs. 4a and 4b. The APs and BD locations are fixed. In Fig. 10, the BF vector for \mathcal{P}_D is obtained by setting the SNR to -25 dB, while in Fig. 11, the BF vector for \mathcal{P}'_D is obtained by setting it to -44.8 dB. These BF vectors are then used to evaluate the resulting performance over a range of SNR values. Similarly, Fig. 12 is an extended version of Fig. 6. In this case, the optimization is performed at an SNR of -25 dB, and the BD location is selected randomly.

The performance of $\mathcal{P}_{\alpha0}$ closely matches that of \mathcal{P}_D , and likewise, the performance of $\mathcal{P}'_{\alpha0}$ is nearly identical to that of \mathcal{P}'_D in Figs. 10 and 11. In Fig. 12, only a negligible difference is observed between the performances of $\mathcal{P}_{\alpha0}$ and \mathcal{P}_D . This similarity arises because, in the given setup, there are sufficient degrees of freedom to completely suppress the DLI while simultaneously focusing the power toward the BD.

In addition, the computational complexity of $\mathcal{P}_{\alpha0}$ is lower than that of \mathcal{P}_D . Moreover, unlike \mathcal{P}_D and \mathcal{P}'_D , which require careful selection of the SNR value during optimization, $\mathcal{P}_{\alpha0}$ and $\mathcal{P}'_{\alpha0}$ operate independently of any SNR information.

REFERENCES

- [1] A. Kaplan, D. P. Osorio, and E. G. Larsson, "Reducing dynamic range in bistatic backscatter communication via beamforming design," *Proc. IEEE Int. Workshop Signal Process. Adv. Wireless Commun.*, Sep. 2024.
- [2] D. A. L. Galappaththige, F. Rezaei, C. Tellambura, and S. Herath, "Link budget analysis for backscatter-based passive IoT," *IEEE Access*, vol. 10, pp. 128 890–128 922, Dec. 2022.
- [3] D. Mishra and E. G. Larsson, "Optimal channel estimation for reciprocity-based backscattering with a full-duplex MIMO reader," *IEEE Trans. Signal Process.*, vol. 67, no. 6, pp. 1662–1677, Mar. 2019.
- [4] J. Kimionis, A. Bletsas, and J. N. Sahalos, "Increased range bistatic scatter radio," *IEEE Trans. Commun.*, vol. 62, no. 3, pp. 1091–1104, Mar. 2014.
- [5] D. T. Hoang, D. Niyato, D. I. Kim, T.-i. Kim, N. Van Huynh, and S. Gong, *Ambient backscatter communication networks*. Cambridge University Press, 2020.
- [6] B. Gu *et al.*, "Breaking the interference and fading gridlock in backscatter communications: State-of-the-art, design challenges, and future directions," *IEEE Commun. Surv. Tutor.*, Jul. 2024.
- [7] T. Jiang *et al.*, "Backscatter communication meets practical battery-free Internet of Things: A survey and outlook," *IEEE Commun. Surv. Tutor.*, vol. 25, no. 3, pp. 2021–2051, May 2023.
- [8] C. Xu, L. Yang, and P. Zhang, "Practical backscatter communication systems for battery-free Internet of Things: A tutorial and survey of recent research," *IEEE Signal Process. Mag.*, vol. 35, no. 5, pp. 16–27, Sep. 2018.
- [9] C. Song *et al.*, "Advances in wirelessly powered backscatter communications: From antenna/RF circuitry design to printed flexible electronics," *Proc. IEEE*, vol. 110, no. 1, pp. 171–192, Nov. 2021.
- [10] F. Rezaei, D. Galappaththige, C. Tellambura, and S. Herath, "Coding techniques for backscatter communications—A contemporary survey," *IEEE Commun. Surv. Tutor.*, vol. 25, no. 2, pp. 1020–1058, Mar. 2023.
- [11] D. Galappaththige, F. Rezaei, C. Tellambura, and A. Maaref, "Cell-free bistatic backscatter communication: Channel estimation, optimization, and performance analysis," *IEEE Trans. Commun.*, May. 2024.
- [12] L. Qu, D. Mishra, and J. Yuan, "Channel estimation protocol for bistatic backscattering using multi-antenna transceiver," in *Proc. IEEE 33rd Annu. Int. Symp. Pers., Indoor Mobile Radio Commun.*, Dec. 2022, pp. 439–444.
- [13] F. Rezaei, D. Galappaththige, C. Tellambura, and A. Maaref, "Time-spread pilot-based channel estimation for backscatter networks," *IEEE Trans. Commun.*, Oct. 2023.
- [14] G. Sacarello, M. Awais, and Y. H. Kim, "Bistatic backscatter NOMA with transmit and receive beamforming," in *Int. Conf. Inf. Commun. Techn. Conver. (ICTC)*, Dec. 2021, pp. 851–853.
- [15] R. Duan, R. Jäntti, H. Yigitler, and K. Ruttik, "On the achievable rate of bistatic modulated rescatter systems," *IEEE Trans. Veh. Technol.*, vol. 66, no. 10, pp. 9609–9613, Jun. 2017.
- [16] S. Zargari, D. Galappaththige, and C. Tellambura, "Refined-deep reinforcement learning for MIMO bistatic backscatter resource allocation," *arXiv preprint arXiv:2405.14046*, 2024.
- [17] X. Jia and X. Zhou, "Power beacon placement for maximizing guaranteed coverage in bistatic backscatter networks," *IEEE Trans. Commun.*, vol. 69, no. 11, pp. 7895–7909, Aug. 2021.
- [18] K. Han and K. Huang, "Wirelessly powered backscatter communication networks: Modeling, coverage, and capacity," *IEEE Trans. Wireless Commun.*, vol. 16, no. 4, pp. 2548–2561, Apr. 2017.
- [19] H. Luan, X. Xie, L. Han, C. He, and Z. J. Wang, "A better than Alamouti OSTBC for MIMO backscatter communications," *IEEE Trans. Wireless Commun.*, vol. 21, no. 2, pp. 1117–1131, Aug. 2021.
- [20] A. Kaplan, D. P. M. Osorio, and E. G. Larsson, "Access point selection for bistatic backscatter communication in cell-free MIMO," in *Proc. IEEE Int. Conf. Commun. (ICC)*, Jun., 2024, pp. 3214–3219.
- [21] A. Varshney *et al.*, "Lorea: A backscatter architecture that achieves a long communication range," in *Proc. ACM Conf. Embedded Netw. Sensor Syst.*, Nov. 2017.
- [22] M. Lopez, N. He, and T. A. Khan, "Designing a bistatic backscatter communications system with OFDM for 6G Internet of Things," in *Proc. IEEE 98th Veh. Technol. Conf. (VTC-Fall)*, Sep. 2023, pp. 1–6.
- [23] D. Li, "Capacity of backscatter communication with frequency shift in Rician fading channels," *IEEE Wireless Commun. Lett.*, vol. 8, no. 6, pp. 1639–1643, Dec. 2019.
- [24] Q. Tao, Y. Li, C. Zhong, S. Shao, and Z. Zhang, "A novel interference cancellation scheme for bistatic backscatter communication systems," *IEEE Commun. Lett.*, vol. 25, no. 6, pp. 2014–2018, Jun. 2021.
- [25] Z. Li, P. Chen, G. Chen, and Y. Fang, "Code index modulated chaotic ambient backscatter communication with differential Walsh codes," *IEEE Wireless Commun. Lett.*, Jan. 2024.
- [26] J. Kan, L. Xiao, Z. Niu, Y. Zhang, and T. Jiang, "Differential modulation-aided practical backscatter communications: Interference cancellation strategy design and implementation," *IEEE Wireless Commun. Lett.*, Sep. 2023.

- [27] R. Biswas *et al.*, “Direct path interference suppression requirements for bistatic backscatter communication system,” in *Proc. IEEE 93rd Veh. Technol. Conf. (VTC-Spring)*, Apr. 2021.
- [28] D. Li, H. Zhang, and L. Fan, “Adaptive mode selection for backscatter-assisted communication systems with opportunistic SIC,” *IEEE Trans. Veh. Technol.*, vol. 69, no. 2, pp. 2327–2331, Dec. 2019.
- [29] M. Rostami, K. Sundaresan, E. Chai, S. Rangarajan, and D. Ganesan, “Redefining passive in backscattering with commodity devices,” in *Proc. 26th Annu. Int. Conf. Mobile Comput. Netw.*, Apr. 2020, pp. 1–13.
- [30] H. Chen, Z. Huang, Y.-C. Liang, and R. Schober, “Multi-antenna broadband backscatter communications,” *arXiv preprint arXiv:2408.08796*, Aug. 2024.
- [31] A. Kaplan, J. Vieira, and E. G. Larsson, “Direct link interference suppression for bistatic backscatter communication in distributed MIMO,” *IEEE Trans. Wireless Commun.*, vol. 23, no. 2, pp. 1024–1036, Feb. 2024.
- [32] A. H. Sayed, *Adaptive Filters*. NJ, USA: John Wiley & Sons, 2011.
- [33] D. H. Brandwood, “A complex gradient operator and its application in adaptive array theory,” in *IEE Proceedings H (Microwaves, Optics and Antennas)*, vol. 130, no. 1. IET Digital Library, 1983, pp. 11–16.
- [34] M. Sarajlić, L. Liu, and O. Edfors, “When are low resolution ADCs energy efficient in massive MIMO?” *IEEE Access*, vol. 5, pp. 14 837–14 853, Jul. 2017.
- [35] E. Björnson, L. Sanguinetti, and J. Hoydis, “Hardware distortion correlation has negligible impact on UL massive MIMO spectral efficiency,” *IEEE Trans. Commun.*, vol. 67, no. 2, pp. 1085–1098, Oct. 2018.
- [36] S. Jacobsson, G. Durisi, M. Coldrey, U. Gustavsson, and C. Studer, “Throughput analysis of massive MIMO uplink with low-resolution ADCs,” *IEEE Trans. Wireless Commun.*, vol. 16, no. 6, pp. 4038–4051, Apr. 2017.
- [37] R. J. Baker, *CMOS: Mixed-Signal Circuit Design*. NJ, USA: Wiley, 2008.
- [38] K. Shen and W. Yu, “Fractional programming for communication systems—part I: Power control and beamforming,” *IEEE Trans. Signal Process.*, vol. 66, no. 10, pp. 2616–2630, May. 2018.
- [39] A. Mezghani and R. W. Heath, “Massive MIMO precoding and spectral shaping with low resolution phase-only DACs and active constellation extension,” *IEEE Trans. Wireless Commun.*, vol. 21, no. 7, pp. 5265–5278, Jan. 2022.
- [40] S. Jacobsson, G. Durisi, M. Coldrey, T. Goldstein, and C. Studer, “Quantized precoding for massive MU-MIMO,” *IEEE Trans. Commun.*, vol. 65, no. 11, pp. 4670–4684, Jul. 2017.
- [41] C. Eckart and G. Young, “The approximation of one matrix by another of lower rank,” *Psychometrika*, vol. 1, no. 3, pp. 211–218, 1936.
- [42] J. Kleinberg and E. Tardos, *Algorithm Design*, Boston, MA, USA: Addison-Wesley, 2011.
- [43] M. S. Lobo, L. Vandenberghe, S. Boyd, and H. Lebret, “Applications of second-order cone programming,” *Linear Algebra and its Applications*, vol. 284, no. 1-3, pp. 193–228, Nov. 1998.
- [44] I. M. Bomze, V. F. Demjanov, R. Fletcher, T. Terlaky, and I. Pólik, “Interior point methods for nonlinear optimization,” in *Nonlinear Optimization*. New York, NY, USA: Springer, 2010, pp. 215–276.
- [45] B. J. B. Deutschmann, T. Wilding, E. G. Larsson, and K. Witrisal, “Location-based initial access for wireless power transfer with physically large arrays,” in *Proc. IEEE Int. Conf. Commun. Workshops (ICC Workshops)*, May 2022, pp. 127–132.